Science Advances

AAAS

advances.sciencemag.org/cgi/content/full/2/9/e1501228/DC1

Supplementary Materials for

Structural basis for KCNE3 modulation of potassium recycling in epithelia

Brett M. Kroncke, Wade D. Van Horn, Jarrod Smith, CongBao Kang, Richard C. Welch, Yuanli Song, David P. Nannemann, Keenan C. Taylor, Nicholas J. Sisco, Alfred L. George Jr., Jens Meiler, Carlos G. Vanoye, Charles R. Sanders

Published 9 September 2016, *Sci. Adv.* **2**, e1501228 (2016)
DOI: 10.1126/sciadv.1501228

The PDF file includes:

- fig. S16. Representative 23 KCNE3-KCNQ1 models based on satisfaction of experimental restraints and Rosetta scoring function.
- fig. S17. Comparison between structurally characterized KCNE family members.
- fig. S18. Sequence conservation within the entire KCNE family and within KCNE3 from different organisms.
- fig. S19. KCNE3 reduces the KCNQ1[Q4S4] current amplitude without reducing channel protein levels at the membrane.
- table S1. Statistics for restraints, structural calculations, and structural quality for the 10 lowest-energy structures of 9764 calculated using XPLOR and further refined in AMBER.
- table S2. KCNQ1-KCNE3 residue pairs predicted to be proximal based on experimental work.
- References (*78–83*)

Other Supplementary Material for this manuscript includes the following:
(available at advances.sciencemag.org/cgi/content/full/2/9/e1501228/DC1)

- PDB coordinates

Supplementary Materials and Methods

Recombinant expression and purification of KCNE3

Human KCNE3 was expressed in *E. coli* in various isotopically-labeled forms and purified as described previously (*59*). Briefly, protein was purified using metal ion affinity chromatography into a buffer containing 250 mM imidazole, pH 6.5, with 2% bicelles (w/v total DHPC+DMPG) containing a lipid-to-detergent molar ratio (q) of 0.33. Samples were then concentrated 10X for NMR. NMR assignments for KCNE3 in DHPC/DMPG bicelles were reported previously (*59*) and are available in the Biological Magnetic Resonance Data Bank (BMRB Entry 16621).

NMR residual dipolar coupling (RDC) measurements for KCNE3 in bicelles

A stretched neutral polyacrylamide gel was used to marginally align uniformly ^{2}H,^{15}N-labeled KCNE3 in bicelles for RDC measurements (*37*). A 6% polyacrylamide gel was cast in a 6.0 mm diameter chamber using an acrylamide/bis-acrylamide (37.5:1 w/w) solution. The gel was washed 2-3× with water followed by soaking in NMR buffer (250 mM imidazole, 2 mM DTT, 0.5 mM EDTA, 6.5, 20% q=0.33 DHPC/DMPG bicelles, and 10% D_2O) overnight. Purified KCNE3 was concentrated to ca. 1 mM in NMR buffer and about 550 µL this solution was incubated with the equilibrated gel for 24 h, allowing much of the protein to diffuse into the gel. The gel was then stretched into an open-ended 4.2 mm inner diameter NMR tube. The remaining solution after soaking the gel also contained KCNE3 and was used as an isotropic reference for the aligned RDC sample. The ^{1}H-^{15}N-RDCs were measured using a uniformly-labeled ^{2}H, ^{13}C and ^{15}N-labeled sample. The RDC data were acquired using interleaved experiments to obtain TROSY and semi-TROSY resonances. The ^{1}H couplings were obtained from the frequency differences between TROSY and semi-TROSY resonances in the aligned and isotropic samples as shown in fig. S3. The NMR spectra were processed using TopSpin and NMRPipe (*64*) and analyzed using NMRview (*65*). In order to avoid potential dynamic structural biases from the

loop regions of KCNE3 only RDCs from the N-terminal α-helix and TM helix were employed in the structure calculations. Dipolar wave analysis of the RDC data was used to qualitatively interpret the data as well as to estimate the associated error of the measurements. The data were fit using an in-house script for QtOctave (fig. S4) (*78*).

Paramagnetic relaxation enhancement (PRE) measurements for bicelle-associated KCNE3

Wild type KCNE3 has one cysteine residue present in the amino acid sequence. A cysteine-less KCNE3 (C31S) was made using site-directed mutagenesis (Agilent) and used as a template for single-cysteine KCNE3 mutants. Four single-cysteine constructs were used for PRE measurements: S13C, S57C, S74C, and S82C. Single cysteine-containing uniformly ^{15}N-labeled (U-^{15}N) KCNE3 mutants were purified as described previously (*37*). After purification, the samples (ca. 0.2 mM KCNE3 dissolved in 300 mM imidazole, 50 mM phosphate pH 7.8, 0.05% LMPG) were incubated with 2.5 mM DTT for at least 3 h. After incubation with DTT, the sample was mixed with 1-oxyl-2,2,5,5-tetramethylpyrroline-3-methyl-methanethiosulfonate (MTSL, Toronto Research Chemicals, Toronto, Canada). MTSL was added to 10 mM from a 250 mM stock solution in acetonitrile and incubated at 37 °C for 3 h, followed by overnight incubation at RT. Samples were then buffer-exchanged using centrifugal ultrafiltration to remove imidazole and re-associated to a Ni^{2+} column. After rebinding, the resin was washed 8-10X with 2 column volumes (16-20 total column volumes) of 0.05% LMPG, 50 mM phosphate (pH 7.8) buffer to remove unreacted MTSL. The resin was then equilibrated with 10 column volumes of 0.5% DHPC in 50 mM phosphate buffer (pH 7.8). Spin-labeled KCNE3 was eluted from the resin in a buffer containing 2% DHPC/DMPG bicelles, 100 mM imidazole (pH 6.5) and concentrated 10X for NMR experiments. Sites for labeling were chosen to represent key structural regions of KCNE3.

PRE data were acquired 40°C at 600 or 800 MHz by recording a sample/parameter-matched paramagnetic vs. diamagnetic pair of 2D ^{1}H-^{15}N TROSY-HSQC experiments (*79*) for each spin-labeled KCNE3 sample. The matched diamagnetic sample was generated by reducing the paramagnetic sample with 20 mM ascorbic acid. The 2-D NMR data were recorded with 64 or 128 scans for each t1 increment and 128 × 1024 complex points in the t1 × t2 dimensions. Spectra were processed using NMRPipe (*64*) and analyzed in SPARKY (*66*) to determine the intensity ratio of the paramagnetic vs. diamagnetic samples. The intensity ratios and diamagnetic sample linewidths were used to determine the PRE contribution to the ^{1}H transverse relaxation rate (R2*). R2* was used to determine the distance between the paramagnetic nitroxide and amide proton using the Solomon and Bloembergen equation, as described previously (*62, 63*). The NMR resonances used to generate structural distance restraints were all well resolved. In addition, distances from probes to sites in loop segments (identified by chemical shift index analysis (*59*); fig. S2), were omitted as a source of PRE-based distance restraints to limit the potential for structural biases that could arise from loop conformational flexibility. Examples of the PRE data are shown in fig. S5.

Mapping of the membrane topology of KCNE3 using water soluble and lipophilic paramagnetic probes

Protein accessibility to lipophilic and aqueous probe data was assessed using data collected at 800 MHz using parameter-matched pairs of 2D ^{1}H-^{15}N TROSY-HSQC for diamagnetic versus paramagnetic samples. Wild type KCNE3 samples were prepared as described above into a final solution of 250 mM imidazole (pH 6.5), 20% bicelles (w/v total DHPC+DMPG) q = 0.33, ca. 0.3 mM KCNE3, 5% D_2O and 10 mM EDTA. The samples were then divided into two fractions, one resuspended with 16 DOXYL-stearic acid (16-DSA, Aldrich, Milwaukee, WI), a lipophilic paramagnetic probe, and the other resuspended with Gd(III)-diethylenetriaminepentaacetic acid (Gd-DTPA, Aldrich), an aqueous paramagnetic probe. Prior to the addition of 20 mM Gd-DTPA,

a reference spectrum was collected without a relaxation enhancement reagent. After the collection of the reference 2-D ^{1}H,^{15}N-TROSY NMR spectrum, 20 mM Gd-DTPA was added, followed by incubation for at least 1 h before collecting a parameter-matched paramagnetic spectrum. The 10 mM free EDTA in the buffer was present to ensure capping any free metal ion sites in the Gd-DTPA chelate, which otherwise might bind transiently and non-specifically to protein carboxyl sites. For samples containing the lipophilic 16-DSA, 113 µL of a 2.5 mg/mL 16-DSA methanol solution was dried for 4 h in a 1.5 mL Eppendorf tube in a rotary evaporator until only a thin 16-DSA residue was left. 0.2 mL of a bicellar KCNE3 solution was then added and incubated overnight at 37 °C before collecting a parameter matched 16-DSA (4 mol% 16-DSA:DMPG) spectrum.

Amide hydrogen-deuterium exchange measurements for KCNE3 in bicelles

^{15}N-Labeled KCNE3 (0.3 mM) samples were prepared as described above into a final 5% D_2O buffer of 250 mM imidazole (pH 6.5), 20% bicelles (w/v total DHPC+DMPG) q = 0.33, followed by a collection of a reference (non-exchanged) TROSY spectrum. Next, 0.2 mL of the KCNE3 solution was diluted 25X with 5 mL of 100% D_2O containing 250 mM imidazole (pH 6.5) and 0.7% DHPC. The sample was then concentrated to 0.2 mL using a 10 kDa MWCO concentrator, re-diluted [5 mL of 100% D_2O, 250 mM imidazole, 0.5 mM EDTA (pH 6.5) and 0.7% DHPC], and re-concentrated to 0.2 mL. These steps took ca. 40 minutes from the first D_2O addition. Acquisition of a TROSY spectrum was initiated and completed after 3 hours. The acquisition parameters were identical between the D_2O-free reference and the post-D_2O addition spectra, with 80 scans per t1 point and 80 points in the indirect dimension.

^{15}N NMR relaxation measurements for KCNE3 in bicelles

Sensitivity- and gradient-enhanced experiments were used to measure HSQC-based T_1, T_2, and ^{15}N-(^{1}H)-NOE parameters on a ^{15}N-labeled KCNE3 sample at 600 MHz (*67, 68*). For T_1

measurements, relaxation delays of 200, 400, 800, 1200, 1600 and 2000 ms were used, with the 200 ms delay repeated to determine experimental error. For T_2 measurements, delays of 0, 9, 17, 35, 69, 138 and 200 ms were employed and the 9 ms delay was repeated. SPARKY software was used to fit the resulting curves. ^{15}N-(^{1}H)-NOE values were measured from the intensity ratios determined from a pair of experiments, one of which included 3 s proton presaturation. All spectra were recorded with 128 X 1024 complex points in the t1 × t2 dimensions, with 32 scans per t1 point. These data are shown in fig. S6. As expected, the two helical segments exhibit more rigidity than the corresponding loop regions.

Structure determination for KCNE3 in bicelles

The structure of full length KCNE3 sequence was determined based on NMR restraints that included the PRE and RDC restraints mentioned above, as well backbone torsion restraints derived from chemical shifts and NOE distance restraints. Backbone C_α, C_β, CO, and N chemical shifts were input into TALOS+ (*60*) to generate backbone dihedral angle restraints. Chemical shift index (CSI) analysis was also used to generate hydrogen bond restraints (*61*). A 3-dimensional (^{1}H,^{1}H,^{15}N)-TROSY-NOESY experiment was carried out on U-^{13}C,^{15}N-KCNE3 (80 ms mixing time) in DHPC/DMPG bicelles in the standard NMR conditions mentioned above to obtain 181 short- and medium-range backbone NOE distance restraints. The PRE restraints were obtained as described above. Briefly, these restraints were classified as close in space if the paramagnetic/diamagnetic intensity ratios were less than 0.15, in which case the paramagnet-amide proton distance was assigned as being <19 Å. Resonances with ratios between 0.15 and 0.85 where converted to distances and given generous errors of ±7 Å, as estimated by the width of the DEER distance distribution. Resonances that exhibited little to no PRE effects (intensity ratios greater than 0.85) were loosely restrained to be >18 Å and >100 Å. The PRE restraints were implemented as NOE-like restraints from the MTSL pyrroline ring nitrogen on a MTSL-labeled cysteine (CYSP residue) to the backbone amide hydrogen (*37, 80*).

RDC and PRE restraints were only used for the N-terminal and transmembrane helices, not for flexible segments.

Structure calculations were conducted within XPLOR-NIH v2.24 (*15*) starting with extended and torsion angle randomized atomic coordinates for KCNE3. Simulated annealing was carried out with 15000 steps at 3500 K with cooling to 100 K. During the temperature cooling ramp, van der Waals (VDW) interaction potentials were increased by varying the VDW force constant from 0.004 to 4 kcal mol^{-1} $Å^{-4}$. Similarly, force constants were increased for the NOE, PRE, and RDC restraints from 1.0 to 30.0 kcal•mol^{-1} $Å^{-2}$, 1.0 to 30.0 kcal•mol^{-1} $Å^{-2}$, and 0.01 to 1.0 kcal mol^{-1} Hz^{-2}, respectively. To avoid potentially biasing steric clashes involving CYSP residues, the VDW forces for CYSP (nitroxide-modified) side-chain atoms were turned off. High temperature simulated annealing was followed by torsion angle and full-atom minimization. During initial stages of structure calculations, it was noticed that the relatively restraint-free loops would frequently occupy space that in the actual sample would be occupied by the bicelle, an unrealistic feature was remedied in structure refinement as listed below (see table S1**)**.

KCNE3 structure refinement

Ten of the top-scoring 1% XPLOR-NIH-generated KCNE3 structures were selected for further structure refinement in an explicit membrane bilayer using restrained molecular dynamics (rMD). The starting structures were chosen subjectively such that only the TM region of KCNE3 is located within the bilayer. These ten representative structures were solvated in an explicit DMPC bilayer using the CHARMM-GUI server. The membrane solvated structure files were then adapted to AMBER format, using the LIPID14 force field

Using AMBER14 on GPUs (*16*), we first minimized each structure for 15000 steps using steepest descent followed by 15000 steps of conjugate gradient minimization, with protein atoms restrained to starting positions. With KCNE3 still restrained to the XPLOR-NIH

coordinates, careful heating of lipid and water to 10 K over 200 steps was performed using constant volume boundary conditions and Langevin dynamics with a rapid collision frequency (10000 ps^{-1}) to make certain that forces/velocities remained stable while any close solvent/solute contacts that potentially remained were resolved. The system was then heated slowly to 100 K over 30000 steps, with constant volume dynamics and collision frequency reset to the standard value of 1. At this point, the time step was increased from 1 fs to 2 fs and the system was heated to 318 K over 200 ps with constant pressure dynamics and anisotropic pressure scaling. Positional restraints for the KCNE3 side-chains were then removed and the system was equilibrated for 5 ns at 318 K, with NMR restraints (NOE and PRE distances/dihedrals) turned on. With water/lipid now fully equilibrated, the system was quickly cooled back down to 100 K and equilibrated for 1 ns with NMR restraints (NOE and PRE distances/Dihedrals/Hbonds) weighted at 300% (no positionally-restrained protein atoms). The entire system was then heated to 200 K and equilibrated for 1 ns, with NOEs/PREs/Dihedral/Hbond NMR restraints at 300% weight. Finally, the system was heated to 318 K and equilibrated for 2 ns while decreasing the NOEs/PREs/Dihedral/Hbond NMR restraint weight from 300% to 100%. Production rMD at 318 K was then conducted at 65 ns, using constant pressure periodic boundary conditions, anisotropic pressure scaling, and NMR restraint weight set to 100%. A representative structure for each of the ten production trajectories was chosen by determining which frame contains the KCNE3 structure that is closest to the mean for that trajectory. The resulting ten representative KCNE3 structures have been deposited to the PDB with the accession code 2NDJ and are illustrated in fig. S7.

Reconstitution of double spin-labeled KCNE3 into LMPC micelles, DMPG/DHPC bicelles and POPC/POPG liposomes for DEER EPR structural studies

Double spin-labeled KCNE3 was prepared by chemically conjugating MTSL to a double cysteine mutant form of KCNE3 (S57C/S82C) via disulfide bonds using the same spin-labeling

procedure as described above for PRE experiments. The efficiency of double spin-labeling of KCNE3 was 90%, as calculated using the spin label concentration determined by CW EPR and the protein concentration as determined by A_{280}. For micellar conditions, double spin-labeled protein was reconstituted into 5% LMPG (as described above for NMR sample preparation) to a protein concentration of 100 μM.

To reconstitute double spin-labeled KCNE3 into DMPG/DHPC bicelles, the spin-labeled protein was eluted from the Ni-NTA column with 2% (w/v) DMPG/DHPC (q = 0.33) bicelle solution containing 250 mM imidazole at pH 6.5. After elution, the protein-containing pool (~4 mL of 13 μM KCNE3) was concentrated 10-fold using an Amicon Ultra-15 Centrifugal Filter (MWCO = 10 kDa). The final bicelle sample contained 130 μM KCNE3, 20% (w/v) DMPG/DHPC (q=0.33), 250 mM imidazole, and 0.5 mM EDTA at pH 6.5.

The first step in preparing lipid vesicles containing double spin-labeled KCNE3 was to mix 100 μL of 500 μM KCNE3 in 0.2% SDS with 200 μL of a SDS/lipid stock mixture (400mM SDS/75mM POPC/25mM POPG), resulting in a clear solution with a protein:lipid molar ratio of 1:400. The SDS/lipid stock solution was prepared using 15-20 cycles of freeze/thawing to ensure complete conversion to clear and transparent mixed micelles. The KCNE3/SDS/lipid mixture was then subjected to extensive dialysis in a Spectra/Por dialysis tube (15 kDa MWCO, Spectrum Laboratories, Inc., CA) to remove SDS. The 4-liter dialysis buffer (50 mM imidazole, 0.5 mM EDTA at pH 6.5) was changed twice a day for 5 days, during which process KCNE3/POPC/POPG vesicles spontaneously formed. The completion of SDS removal was indicated by the formation of the cloudy KCNE3/lipid liposomes and the increase of the surface tension of the dialysate. The KCNE3/lipid vesicle solution was then extruded through a 100 nm filter to generate unilamellar vesicles using an Avanti Mini-Extruder (Avanti Polar Lipids, Inc., AL).

Four-pulse DEER measurements and data analysis to determine distances between spin labels on opposite ends of the KCNE3 transmembrane domain

Four-pulse DEER experiments were performed using an X-band (9.5 GHz) Bruker spectrometer (ELEXSYS E580) equipped with a Bruker split ring resonator (ER 4118X-MD5) at 80 K employing an Oxford CF935 cryostat coupled with an Oxford ITC4 temperature controller. Double spin-labeled KCNE3 was reconstituted into LMPC micelles, DMPC/DHPC bicelles, or POPC/POPG vesicles prepared as described above, with a final spin label concentration of 150 to 250 μM (1.8X the KCNE3 concentration). Glycerol was added to each sample to 30% (w/w) to serve as a cryoprotectant. Samples were transferred into quartz capillaries with an inner diameter of 2.4 mm (Wilmad LabGlass, Buena, NJ). The experiment was initiated after waiting for the temperature to stabilize at 80 K. A standard four-pulse sequence was employed with a 32 ns π pulse and a 16 ns $\pi/2$ pulse (*69*). All DEER data were analyzed using GLADD (*70*) that simultaneously fits the background signal as a function of both the effective spin concentration and the radius of the molecule, while fitting the dipolar wave with a Gaussian distance distribution.

Mammalian cell cultures

Chinese hamster ovary cells (CHO-K1, CRL 9618, American Type Culture Collection, Rockville, MD, USA) were grown in F-12 nutrient mixture medium (GIBCO/Invitrogen, San Diego, CA, USA) supplemented with 10% fetal bovine serum (FBS, ATLANTA Biologicals, Norcross, GA, USA), penicillin (50 units·mL^{-1}), streptomycin (50 μg·mL^{-1}) at 37°C in 5% CO_2. Unless otherwise stated, all cell culture media was obtained from Life Technologies, Inc. (Grand Island, NY, USA).

Transfection of plasmids into mammalian cells

cDNAs for full-length human KCNQ1 (GenBank accession # AF000571), KCNQ4 (AF105202), and KCNE3 (AF302494) were engineered into the mammalian expression vectors pIRES2-EGFP (KCNQ1 and KCNQ4; BD Biosciences-Clontech, Mountain View, CA, USA) and into a modified pIRES2-vector in which EGFP cDNA was substituted with that of DsRed-MST (pIRES2-DsRed-MST, KCNE3), as previously described (*71, 72*).

KCNQ1-KCNQ4 transmembrane domain chimeras were generated by megaprimer PCR of whole plasmids (MEGAWHOP). The target cDNA region was PCR-amplified using oligonucleotides including a ~10-20 bp region in the 5' end of overlap with the destination plasmid to create two complementary mutagenic megaprimers (~100bp long). The megaprimer product was gel purified and isolated using a QIAQuick gel extract kit (QIAGEN Inc. Valencia, CA, USA). Whole plasmid PCR was then performed using the generated megaprimers to create channel chimera cDNAs sans ligation, encoding forms of KCNQ1 with transmembrane helices from KCNQ4 swapped in. Single mutations were introduced into KCNQ1, KCNQ4 and KCNE3 using the QuikChange Site-Directed Mutagenesis system (Agilent Technologies, Inc., Santa Clara, CA, USA). All recombinant cDNA genes were sequenced to confirm the presence of the desired modifications and the absence of unwanted mutations.

Expression of KCNQ1/4 and KCNE3 constructs in CHO-K1 cells for electrophysiology was achieved by transient plasmid transfection using FUGENE-6 (Roche, Indianapolis, IN, USA) in which 1 µg of KCNQ1/4 cDNA was co-transfected with 1 µg of KCNE3 cDNA. When the pore-forming subunit was expressed in the absence of KCNE3, the cells were co-transfected with the nonrecombinant pIRES2-DsRed-MST empty vector. After transfection, cells were incubated for 48 h before use in electrophysiological or biochemical experiments.

Quantitation of KCNQ1 and related channels in CHO cells

All cell biochemical experiments to determine KCNQ1 channel concentration including the preparation of cellular lysates, immunoprecipitation, and western blotting were completed as described previously (*71, 73*). Briefly, 48 h post-transfection KCNQ1/4-expressing CHO-K1 cells (60 mm dishes) were washed twice with Dulbecco's PBS supplemented with $CaCl_2$ and $MgCl_2$ and incubated with 1.5 $mg \cdot ml^{-1}$ membrane-impermeant sulfo-NHS-biotin reagent (Pierce Chemical Co., Rockford, IL, USA) for 1 h on ice. Cells were then washed 2× with PBS + glycine (100 mM) and incubated for 10 min in PBS + glycine on ice. The cells were lysed with 500 µL RIPA buffer (150 mM NaCl, 50 mM Tris-Base, pH 7.5, 1% IGEPAL, 0.5% sodium deoxycholate, 0.1% SDS) supplemented with a Complete Mini Protease Inhibitor tablet (Roche), centrifuged at 14,000×*g* for 30 min at 4 °C, and the supernatant fraction was retained. Total protein in these lysates was quantified using the Bradford reagent (Bio-Rad Laboratories, Hercules, CA, USA), and equal amounts of proteins (~600 µg) were used in the subsequent immunoprecipitation experiments. The lysates were incubated with ImmunoPure Immobilized Streptavidin beads (50 µL, Pierce Chemical Co.) overnight at 4 °C. The samples were centrifuged for 10 s at 10,000×*g* then washed 3 times with RIPA buffer at 4 °C. The biotinylated proteins were eluted with 57 µL Laemmli sample buffer (Bio-Rad Laboratories) supplemented with 5% 2-mercaptoethanol (β-ME) for 30 min at room temperature (RT, 20–23°C). Western blot analysis was performed by incubation for 1 h at RT with anti-KCNQ1 (goat polyclonal antibody, Santa Cruz, CA, USA) diluted 1:200 for KCNQ1 or the KCNQ1(Q4S4) chimera, or anti-calnexin (rabbit polyclonal antibody, Santa Cruz) diluted 1:500 as a control for biotinylated membrane proteins. Immunoreactive bands were visualized by 1 hr incubation with horseradish peroxidase-conjugated secondary antibodies, rabbit anti-goat for KCNQ1 (diluted 1:10,000, Santa Cruz) and goat anti-rabbit for calnexin (diluted 1:10,000, Santa Cruz). Densitometry of protein bands was used to quantify protein levels (ImageJ software; National Institutes of Health). The KCNQ1 band intensity was compared to the transferrin band to normalize for protein loading.

Electrophysiology of KCNQ1 channel function

On the day of the experiment, transfected cells were dissociated by brief exposure to trypsin/EDTA, resuspended in supplemented F-12 nutrient mixture medium, plated on glass coverslips and allowed to recover for ~2 h at 37 °C in 5% CO_2. Only yellow fluorescent cells (i.e., positive for both EGFP [successful KCNQ1/4 transfection] and DsRed-MST fluorescence [successful KCNE3 transfection]) were studied. Whole-cell currents were recorded at RT using Axopatch 200 or 200B amplifiers (Molecular Devices Corp., Sunnyvale, CA, USA) using the whole-cell configuration of the patch clamp technique (*74*). Pulse generation was conducted with Clampex 8.0 (Molecular Devices Corp.) and whole-cell currents were filtered at 1 kHz and acquired at 5 kHz. Whole-cell currents were not leak-subtracted. Whole-cell currents were measured from -80 to +60 mV in 10 mV steps for 1.99 s after the start of the voltage pulse from a holding potential of –80 mV. The external bath solution contained the following (in mM): NaCl 132, KCl 4.8, $MgCl_2$ 1.2, $CaCl_2$ 1, glucose 5, HEPES 10, pH 7.4. The internal solution contained the following (in mM): K^+ aspartate 110, $CaCl_2$ 1, HEPES 10, EGTA 11, $MgCl_2$ 1, K_2ATP 5, pH 7.3. The pipette solution was diluted 5-10% to prevent activation of swelling-activated currents. Patch pipettes were pulled from thick-wall borosilicate glass (World Precision Instruments, Inc., Sarasota, FL, USA) with a multistage P-97 Flaming-Brown micropipette puller (Sutter Instruments Co., San Rafael, CA, USA) and heat-polished with a Micro Forge MF 830 (Narashige, Japan). After heat polishing, the resistance of the patch pipettes was 3-5 MΩ in the control recording solutions. As a reference electrode, a 2% agar-bridge with a composition similar to the control bath solution was utilized. Junction potentials were zeroed with the filled pipette in the bath solution. Unless otherwise stated, all chemicals were obtained from Sigma-Aldrich (St. Louis, MO, USA).

The association/interaction between KCNQ1 and KCNE3 was analyzed by mutating KCNQ1 and KCNE3 residues to cysteine and testing whether they were close enough to form disulfide

bonds by perfusing the cells with 10 mM DTT (a thiol-based reducing agent) or 100-350μM Cu(II)-phenanthroline (Cu-phen, a disulfide-promoting oxidative catalyst) and then recording whole-cell currents as described above.

The estrogen sensitivity of the wild-type or mutant KCNQ1-KCNE3 channel complex was analyzed by perfusing transfected cells with 100 μM 17β-estradiol or vehicle alone (ethanol, 10 ul/ml) for 4 minutes before whole-cell currents were recorded.

Electrophysiological data analysis

Data were collected for each experimental condition from at least 3 transient transfections and analyzed and plotted using a combination of Clampfit (Molecular Devices Corp.) and SigmaPlot 2000 (Systat Software, Inc., San Jose, CA USA). Statistical analyses were carried out using SigmaStat 2.03 (Systat Software, Inc.) and *p*-values are listed in the figure legends. Whole-cell currents were normalized for membrane capacitance and results are expressed as mean ± SEM. The number of cells used for each experimental condition is specified in the figure legends.

Homology/Rosetta modeling of KCNQ1

The sequence of the KCNQ1 channel transmembrane domain (S0-S6, residues 100-370) was threaded through the K_v1.2/2.1 chimera crystal structure (PDB 2R9R) based on a sequence alignment by CLUSTAL W (*81*). Transmembrane segments for KCNQ1 were predicted using the OCTOPUS web server (http://octopus.cbr.su.se/) (*82*), manually verified to ensure transmembrane segments matched those predicted by sequence alignment with PDB 2R9R, and used to impose membrane-specific energy terms on residues within a theoretical membrane bilayer. Imposing both a membrane-specific score function and C4 symmetry, gaps in the threaded KCNQ1 monomer model resulting from unresolved regions in the template structure or insertions/deletions in the sequence alignment were reconstructed using fragment

insertion (fragments generated by the robetta server; www.Robetta.org) and the cyclic coordinate descent (CCD) algorithm with subsequent iterative sidechain packing and backbone torsion angle minimization from the looprebuild application of Rosetta 3.2. From twenty thousand models generated, the best scoring 1,000 models that kept the selectivity filter and S6 helix (residues 304-348) within 1 Å RMSD of the template structure were energy minimized through 10 iterative side-chain repacking and gradient-based minimization with a ramping repulsive potential (relax) while enforcing an open pore through pseudo restraints of 15.4 Å between residues 349 from different subunits. The best scoring 1,000 models of the relaxed set that satisfied the selectivity filter were subjected to a repeated round of relaxation and it was observed that the improvement in Rosetta energy score was less than 5%. The best scoring 1,000 models that satisfied the selectivity filter and residue 349 restraints were clustered into families with at least 20 members. The lowest energy structures from each family (22 in total) and the best scoring structure from the initial loop rebuilding step were used for subsequent KCNE3 docking steps (section below). MolProbity analysis of the top scoring representative structure indicated 1044 (97.39%) residues in favored regions of the Ramachandran plot, and all residues within allowed regions. MolProbity also reported a clashscore of 2 (99th percentile), 12 poor rotamers (1.32%), no Cβ deviations, 12/8848 (0.14%) bad backbone bonds, and 20/12012 (0.17%) bad backbone angles. The overall MolProbity score is 1.18 (99th percentile). The lowest energy structure from the final ensemble of structures was chosen as the "representative structure" used for making fig. S11.

Docking of KCNE3 to KCNQ1

For the initial docking step, only the membrane spanning segments of KCNQ1 (residues 100-116, 119-145, 154-178, 196-218, 222-286, 299-370) and KCNE3 (residues 56-84) were used. Each of the 10 lowest-energy NMR-derived KCNE3 structures was placed near of the transmembrane region of the 23 representative homology models of KCNQ1, resulting in 230

non-contacting, starting complexes. The membrane center and normal were fixed relative to the KCNQ1 channel and KCNE3 was allowed to translate and rotate during docking. Each of the 230 starting complexes was docked 100 times in two stages: the first stage was a low-resolution, “centroid” docking step with average translational and rotational allowances of 3 Å and 8°, respectively; the second stage consisted of full-atom docking steps where KCNE3 was allowed to translate and rotate an average of 0.1 Å and 1°, respectively, followed by iterative side-chain and backbone optimization. The resulting models were filtered based on a sum of experimental distance-restraint violations squared (table S2). Of the remaining models, the best scoring 1,000 structures were used to reseed a subsequent iteration of docking to generate an additional 25,000 model complexes. The Rosetta scores of the interface between KCNQ1 and KCNE3 used to evaluate model complexes were calculated as KCNE3 was translated 100 Å along the X-axis (within the plane of the membrane), allowing the contacting side-chains at the interface to re-optimize. The total Rosetta score (calculated using the full-atom, membrane-specific score function) of each individual binding partner was then subtracted from the total score of the complex. Subsequent docking iterations were performed with a reduction in average translation and rotation of the “centroid” step perturbation of KCNE3 by a factor of three to 1 Å and 2.8 degrees, respectively. The resulting models were scored, filtered based on experimental distance restraints (table S2) to remove all models that had an atom pair constraint violation sum (a_p_c) greater than 250, and used to reseed another round of docking. Distance restraint scores (a_p_c) were calculated as the sum of the squares of the deviations from the maximal allowed distance in table S2 (plotted in the color axis in figs. S14-15**)**. These steps were iterated until the change in interface energy from iteration to iteration converged to less than 5%.

Once the convergence criterion was met, the flexible extramembrane regions of KCNE3 (residues 51-56) and KCNQ1 (residues 144-155, 177-197, 217-223, and 285-300) were rebuilt

and refined using the cyclic coordinate descent (CCD) and kinematic closure (KIC) methods, respectively, which were energy-minimized, with restraints applied, within the looprebuild module of Rosetta resulting in 19,013 structures. Representative structures were chosen by clustering the 1000 best scoring, loop rebuilt/relaxed structures, followed by selection of the lowest energy member from each family cluster with more than 20 members.

Supplementary Figures

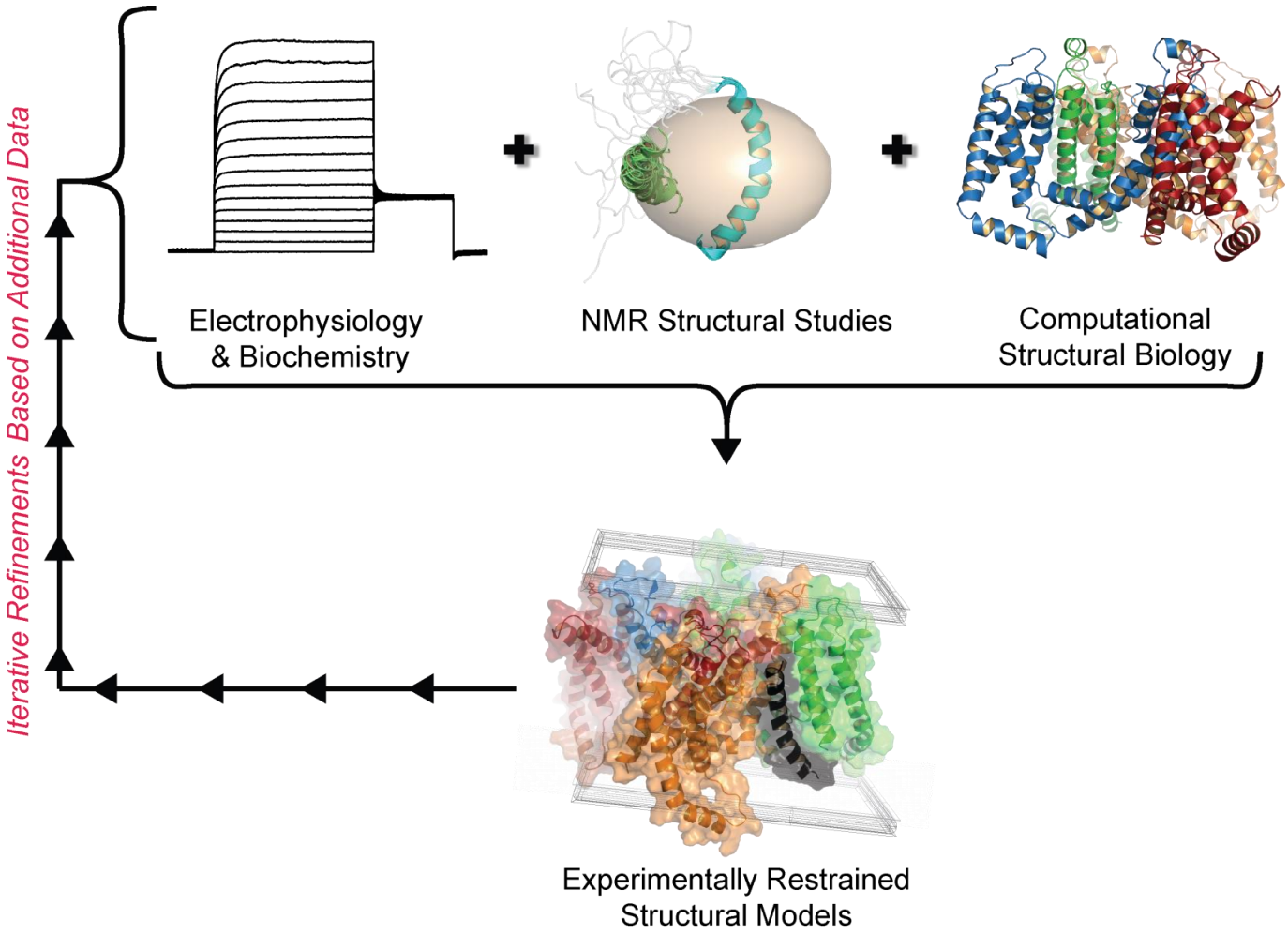

fig. S1. Integrative structural biology to generate experimentally restrained structural models of the KCNE3/KCNQ1channel complex. Combining electrophysiology results with the KCNE3 NMR structure and homology models of KCNQ1 provides a path to forge experimentally-restrained structural models of this ion channel complex. One of the benefits of this experimental design is that the integrative structural models can then be verified and refined by further rounds of experiments as was carried out in the present study. (Figure adapted from (*26*)).

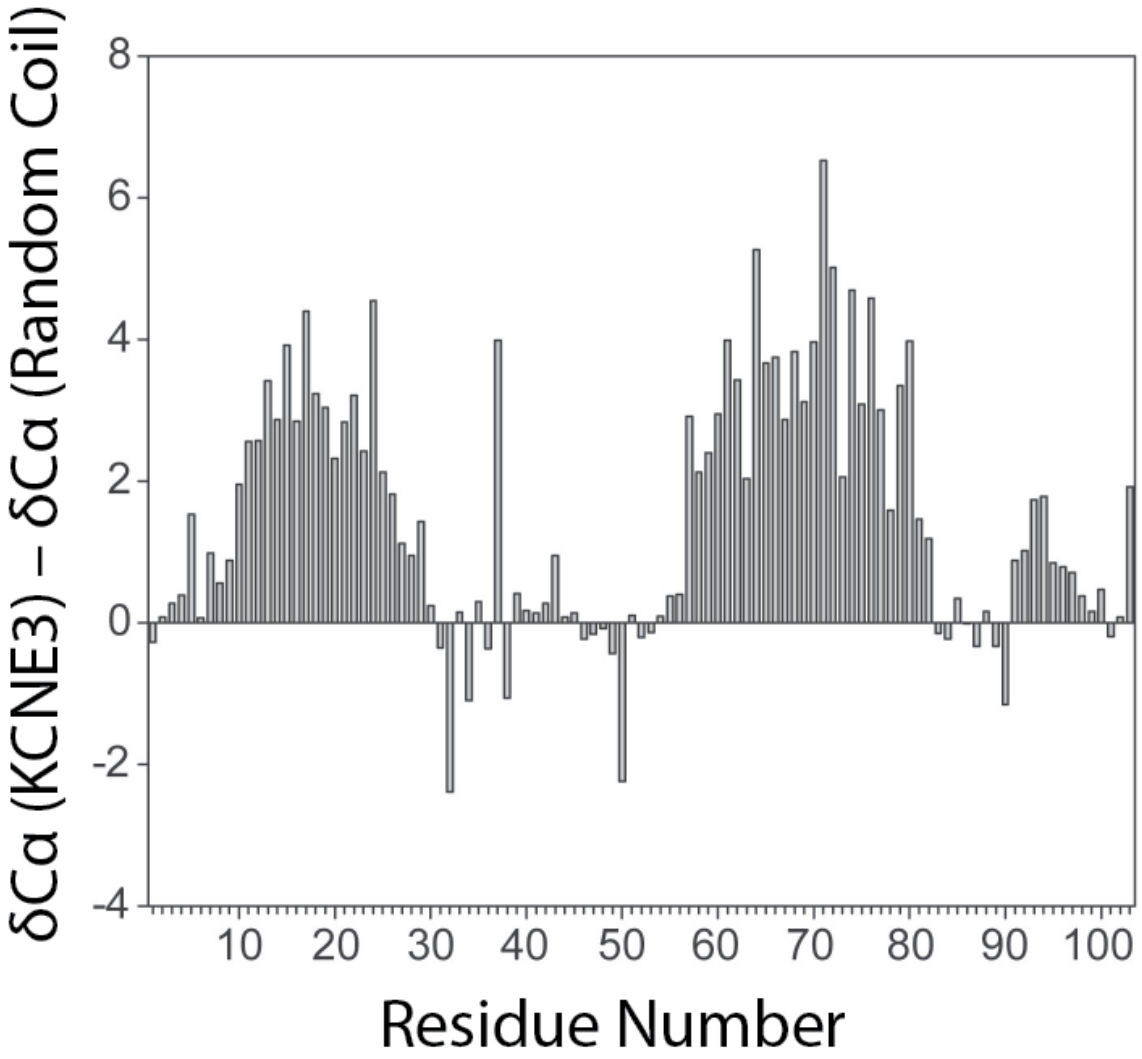

fig. S2. Chemical shift index analysis for KCNE3 in bicelles. Comparison of the NMR chemical shifts of KCNE3 with random coil values allow for accurate determination of the KCNE3 secondary structure. The C_α shifts shown indicate that KCNE3 is comprised of three helices as indicated by positive deflections in the plot.

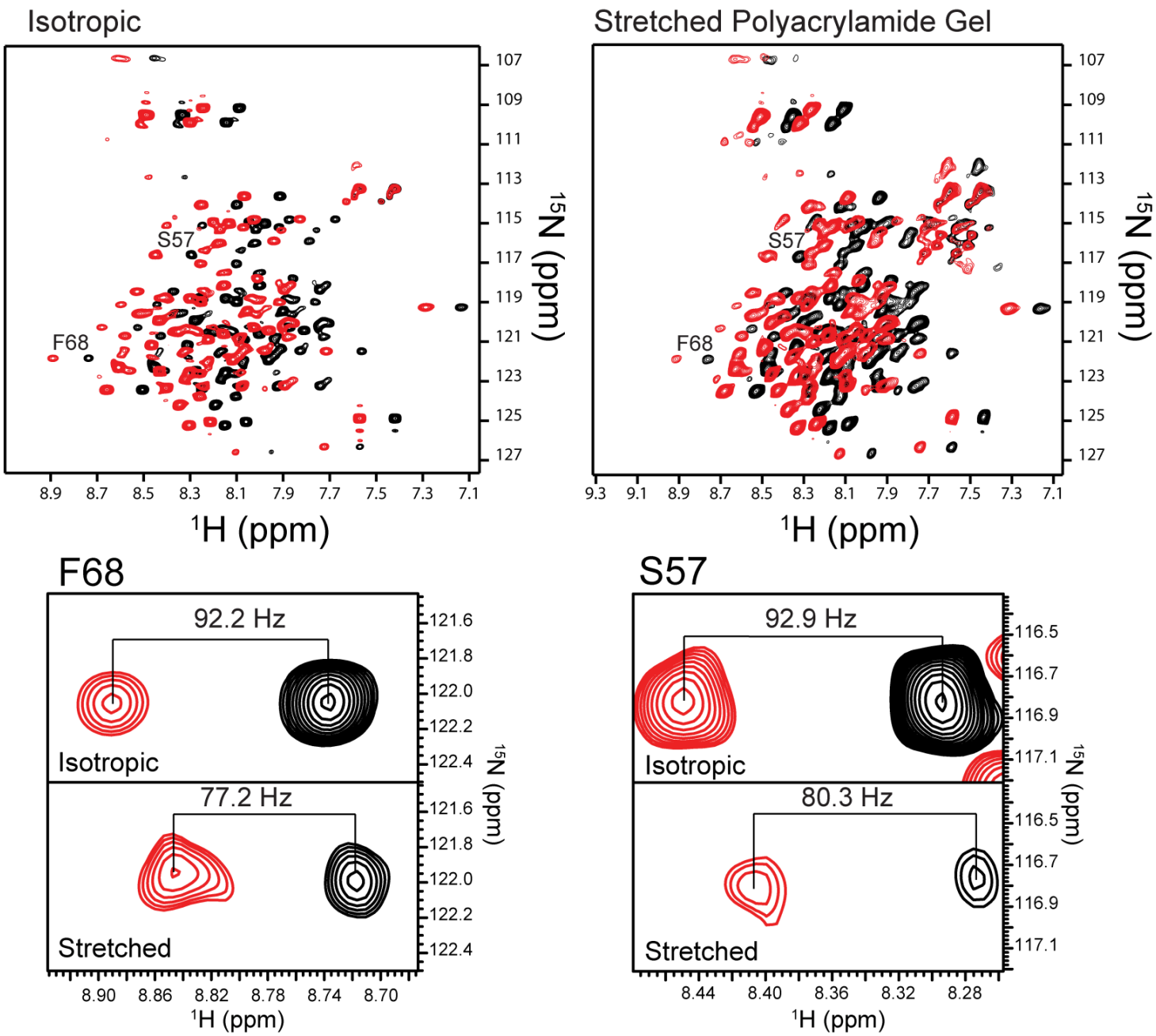

fig. S3. RDC NMR data for KCNE3 in bicelles. The top panels are ^{1}H-^{15}N TROSY HSQC spectra of KCNE3 in both a 6% stretched polyacrylamide gel (aligned sample) and in a gel-free solution (istropic sample). The data were collected at 600 MHz ^{1}H, using U-^{2}H,^{13}C,^{15}N-KCNE3 in standard sample conditions (3:1 molar ratio of ca. 20% DMPC/DMPG/DHPC bicelles, pH 6.5 at 40°C). The bottom panels illustrate the measurement of RDC values for F68 and S57 respectively from the superimposed TROSY (black) and semi-TROSY (red) resonances. These data were used to generate orientational restraints implemented in the NMR structure calculation.

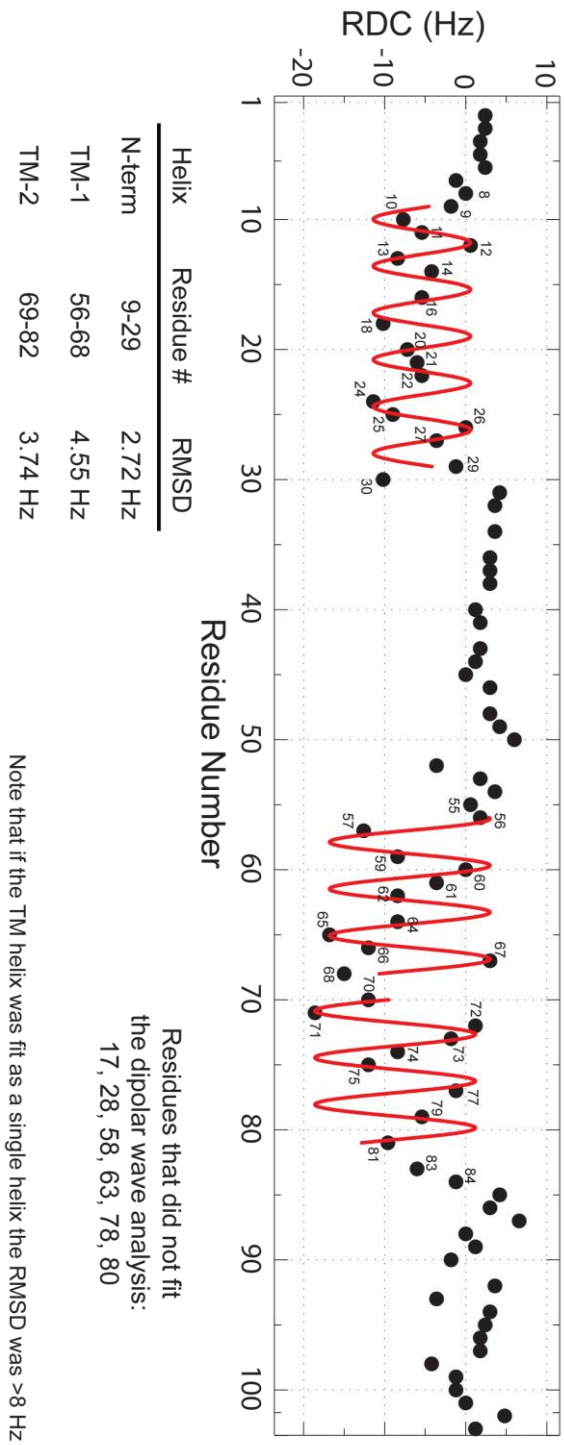

fig. S4. Dipolar wave analysis of bicellar KCNE3 ^{1}H-^{15}H RDCs. RDCs were plotted as a function of residue number and fit to the periodicity of an α-helix to generate the illustrated dipolar wave analysis. The RDC corroborate the CSI data shown in fig. S2, and also reveals that the transmembrane helix is irregular near the center. This irregularity is borne out in the KCNE3 structure and in molecular dynamics simulations.

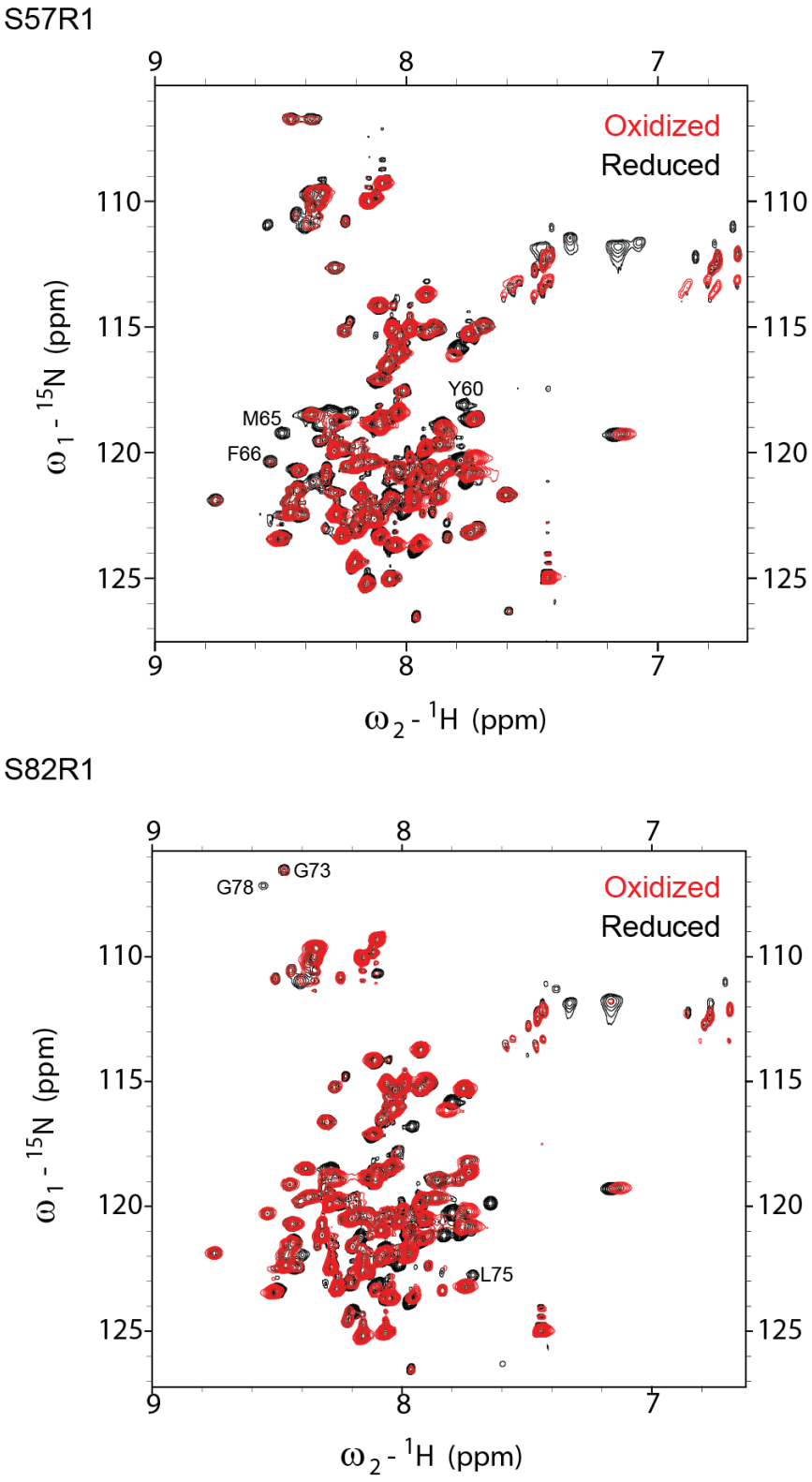

fig. S5. Examples of PRE NMR data for KCNE3 in bicelles. Four cysteine sites were individually spin-labeled with MTSL to generate long-range distance restraints used in structure determination. The diamagnetic (reduced sample) spectra are in black with the paramagnetic spectra shown in red. These data were collected at 600 MHz, 40°C, and pH 6.5 with KCNE3 solubilized in DMPG/DHPC bicelles. After the paramagnetic spectrum was collected, the samples were incubated with 20 mM ascorbic acid for at least one hour to reduce the spin label, generating the diamagnetic sample.

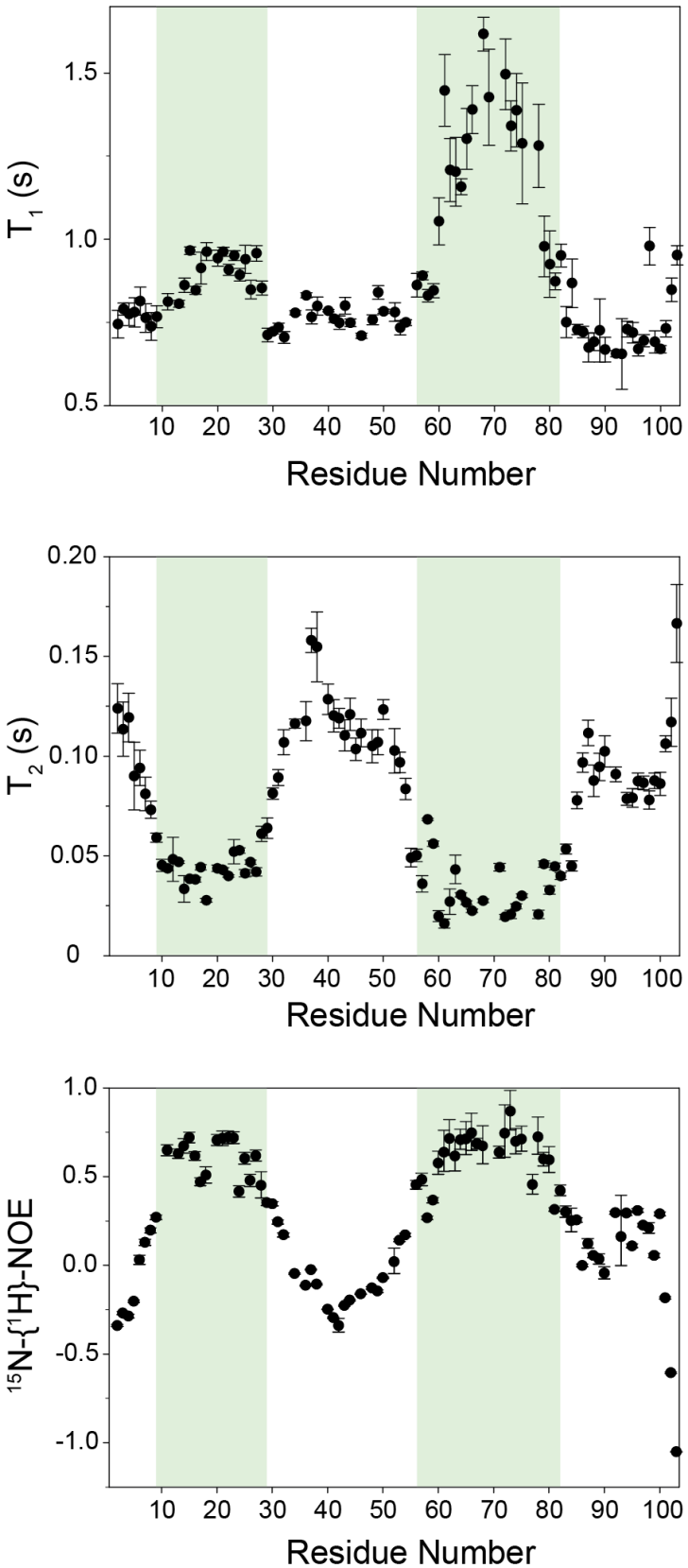

fig. S6. ^{15}N NMR relaxation measurements for KCNE3 in bicelles. Relaxation times and steady-state NOEs are plotted as a function of residue number. The larger structured helices are highlighted with a grey background and can be distinguished by the relatively high T_1 and NOE values and by low T_2 values.

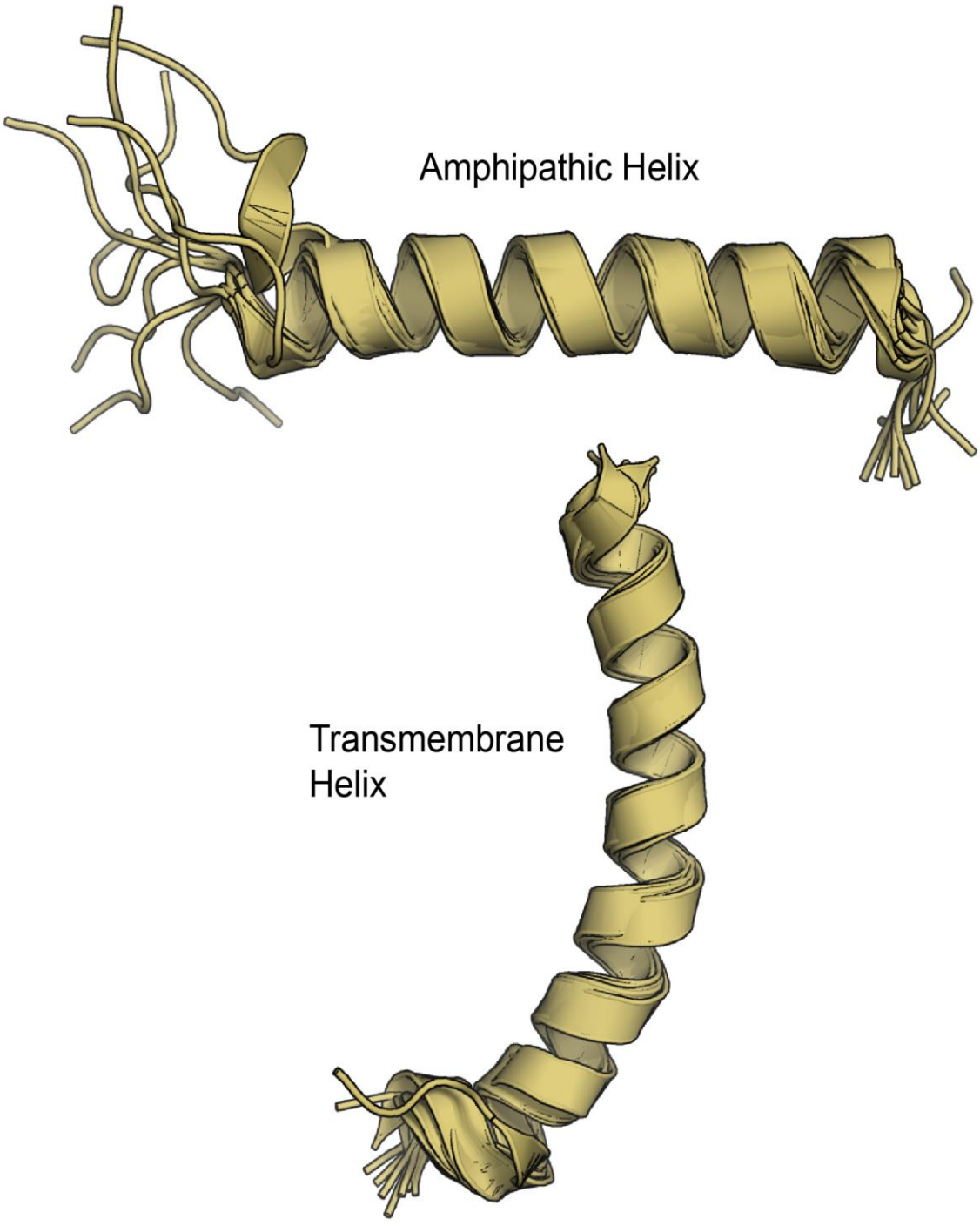

fig. S7. Representative structures of KCNE3 amphipathic and transmembrane helices from AMBER restrained molecular dynamics (rMD) simulations. A representative structure from each of ten rMD refinements was chosen by computing the KCNE3 structure that is closest to the mean during the final 53 ns of production rMD. The degree of overlap highlights the convergence of structured regions within KCNE3.

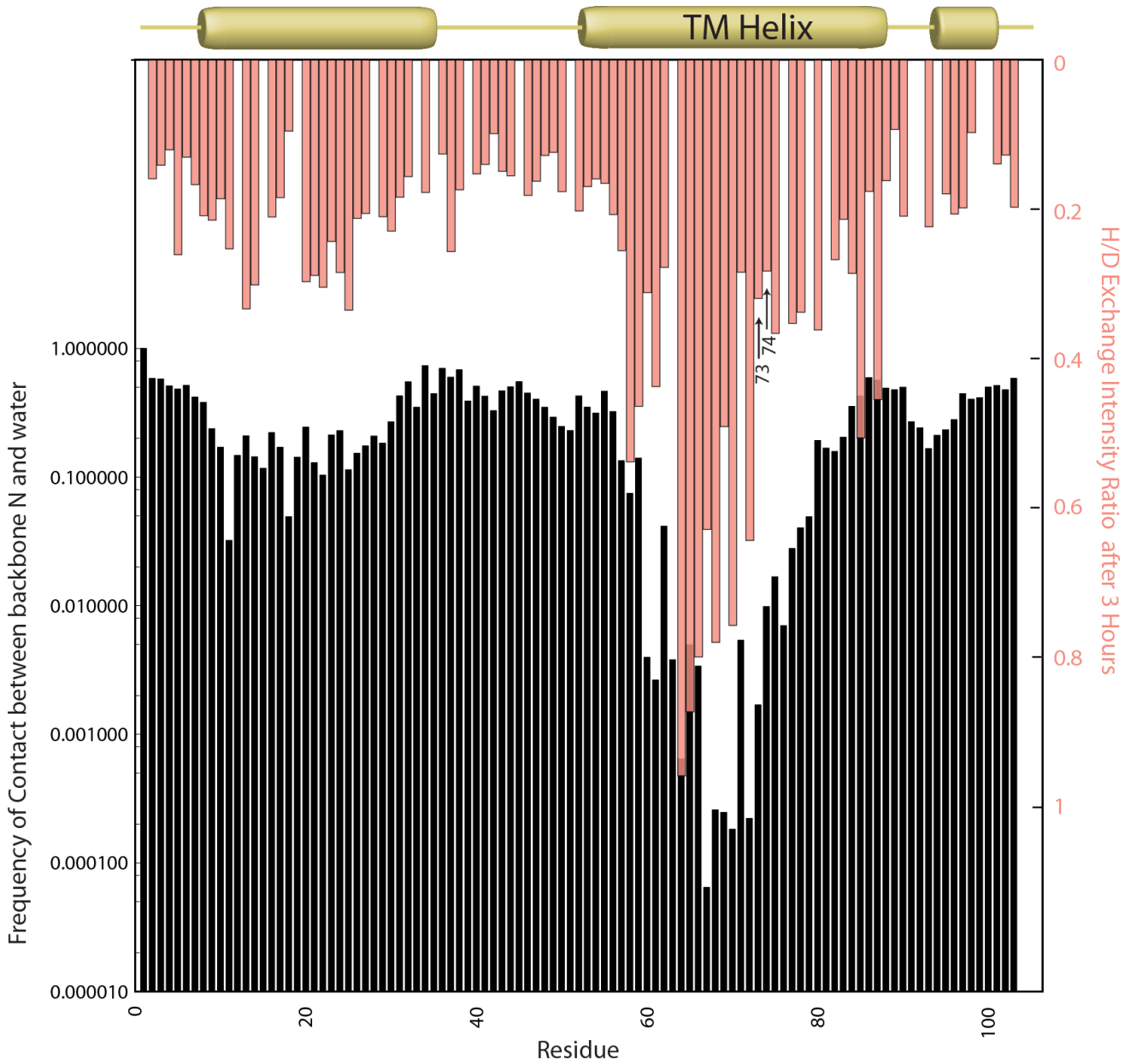

fig. S8. Water access to the TMD of KCNE3. *Shown in the upper part of this figure is the reduction in bicellar WT KCNE3 $^{1}H,^{15}N$-TROSY peak intensities following three hours of hydrogen/deuterium exchange following addition of 100% D_2O. The bottom part of this panel illustrates the frequency of contacts between backbone nitrogens and water as observed during rMD.* It is notable that the amide protons for residues G73 and S74, at nearly the center of the membrane, and also the C-terminal half of the TMD exchange relatively rapidly with D_2O.

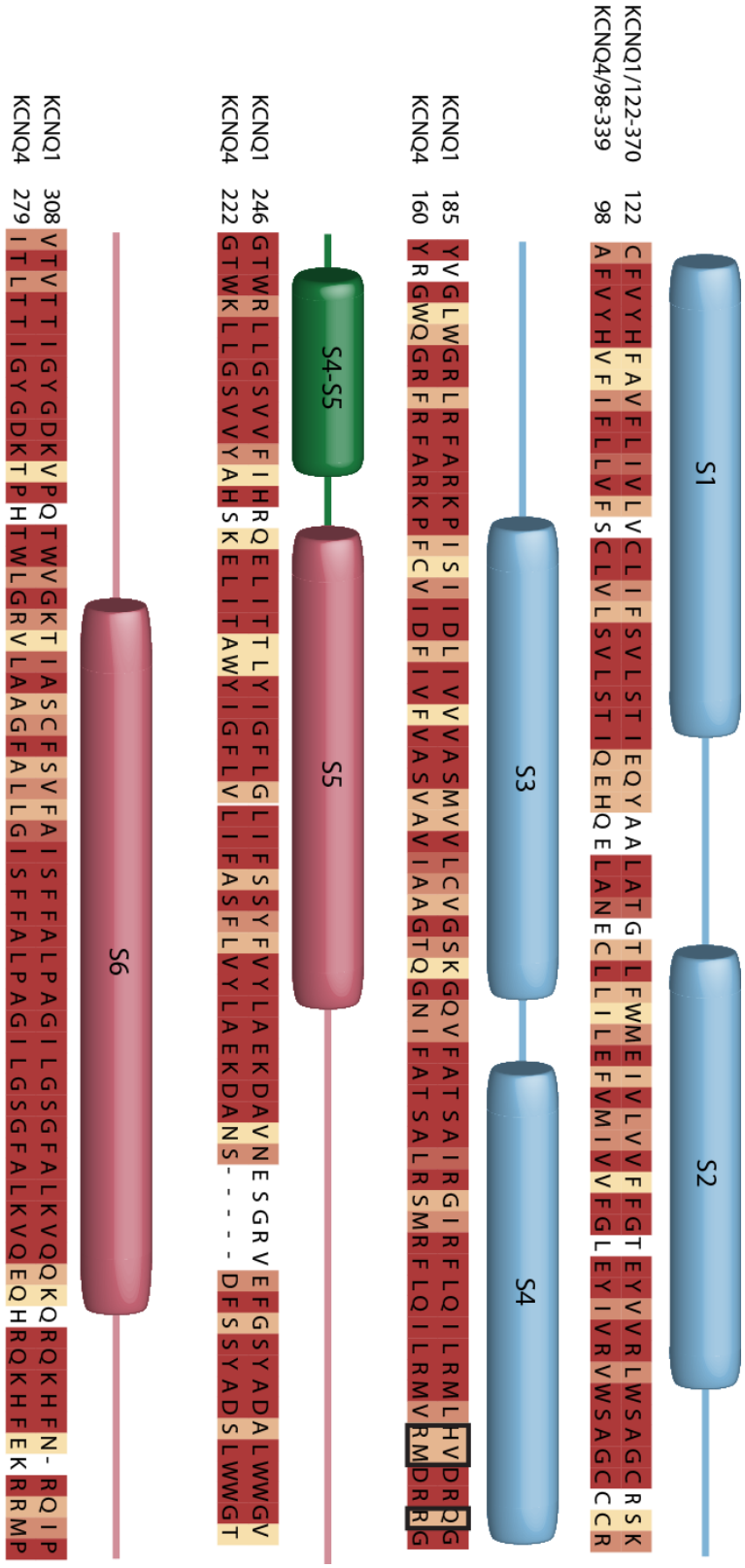

fig. S9. Sequence conservation between KCNQ1 and KCNQ4. Sequence boxes are color coded from white to dark red to reflect the range from divergent to conserved residues. Corresponding to the color scheme used throughout this publication the voltage-sensor domain, S4-S5 linker, and pore domain are colored light blue, green, and red, respectively. The residues found necessary and sufficient to define the KCNE3 modulation profile of KCNQ1 are boxed in black.

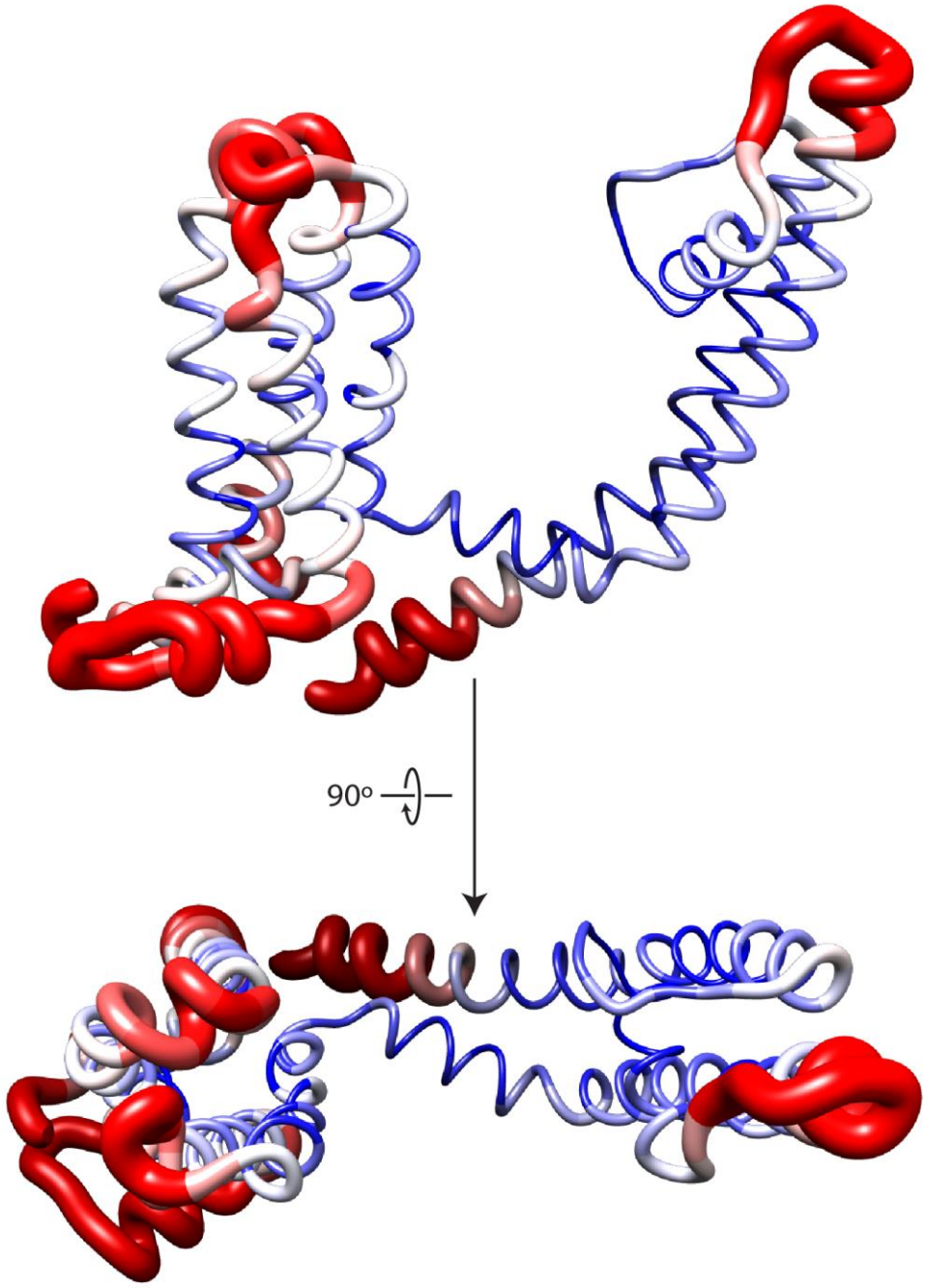

fig. S10. Homology modeling of the open state of KCNQ1. Single monomer of KCNQ1 with α-carbon rmsd between representative 23 models plotted as tubes, with increasing thickness corresponding with increasing per residue α-carbon rmsd. Structures were also color coded to reflect per residue α-carbon rmsd changes from ≤2.0 Å (blue) to ≥5.0 Å (red). The greatest variability falls, not surprisingly, in the linker regions between transmembrane helices and the cytosolic C-terminus of the S6 helix.

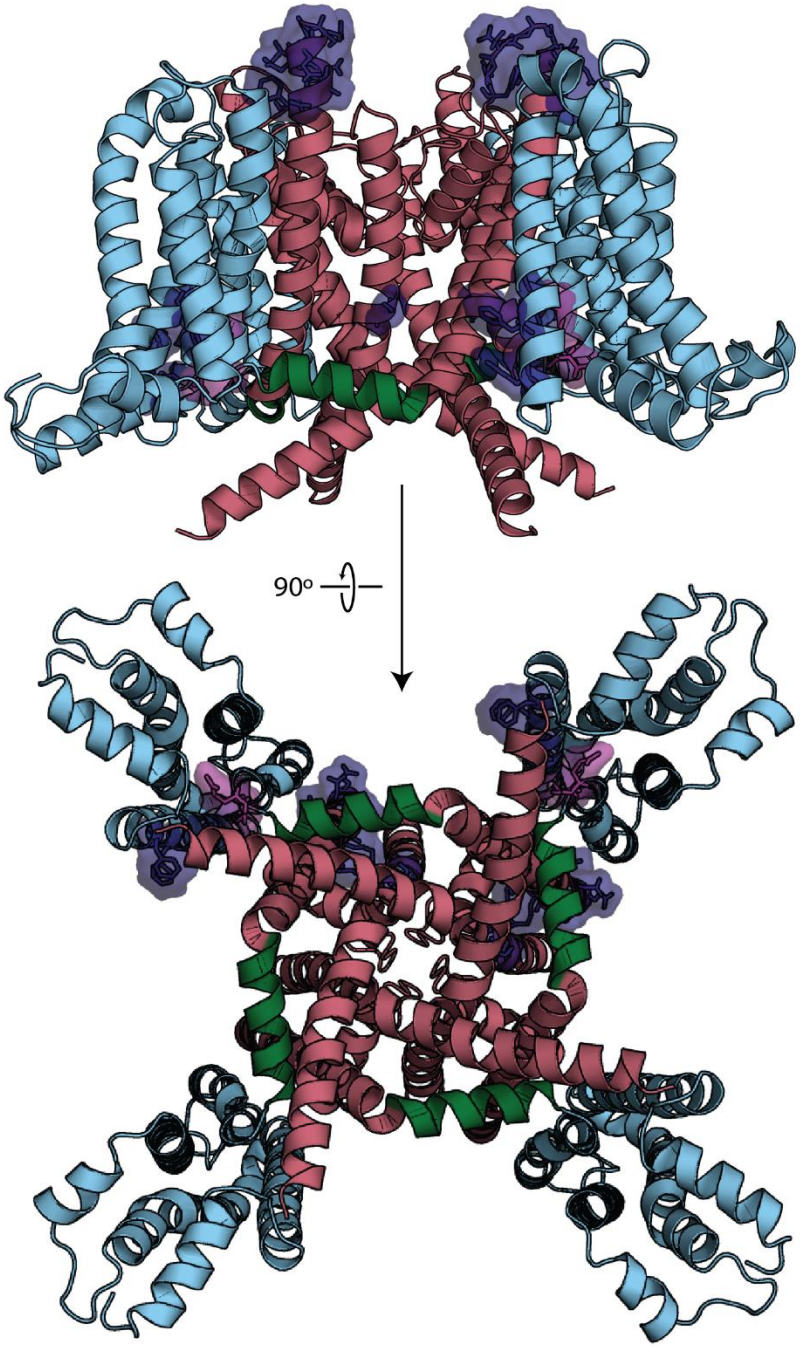

fig. S11. Homology/Rosetta modeling of the KCNQ1 channel open state. Rosetta 3.5 was used to construct structural models of the open (activated) state of the KCNQ1 homotetramer. The three domains of KCNQ1 are colored light blue, green, and red for each monomer's voltage sensor domain, S4-S5 linker, and pore domains, respectively. Residues previously shown to be critical to KCNE3 function are shown in dark blue, while residues found to be important in this study are shown in magenta.

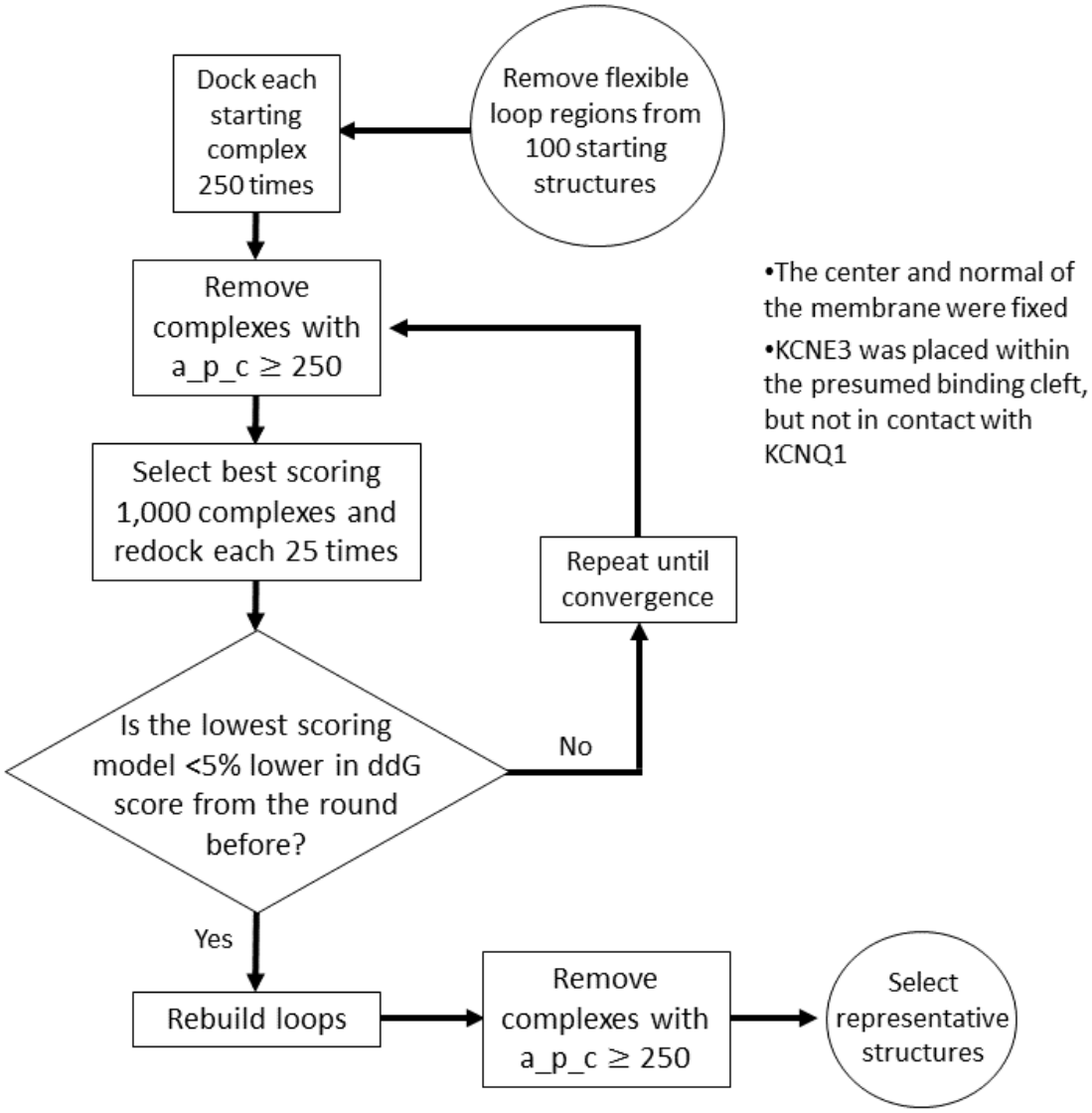

fig. S12. Flowchart displaying the process used to dock KCNE3 to open-state KCNQ1.

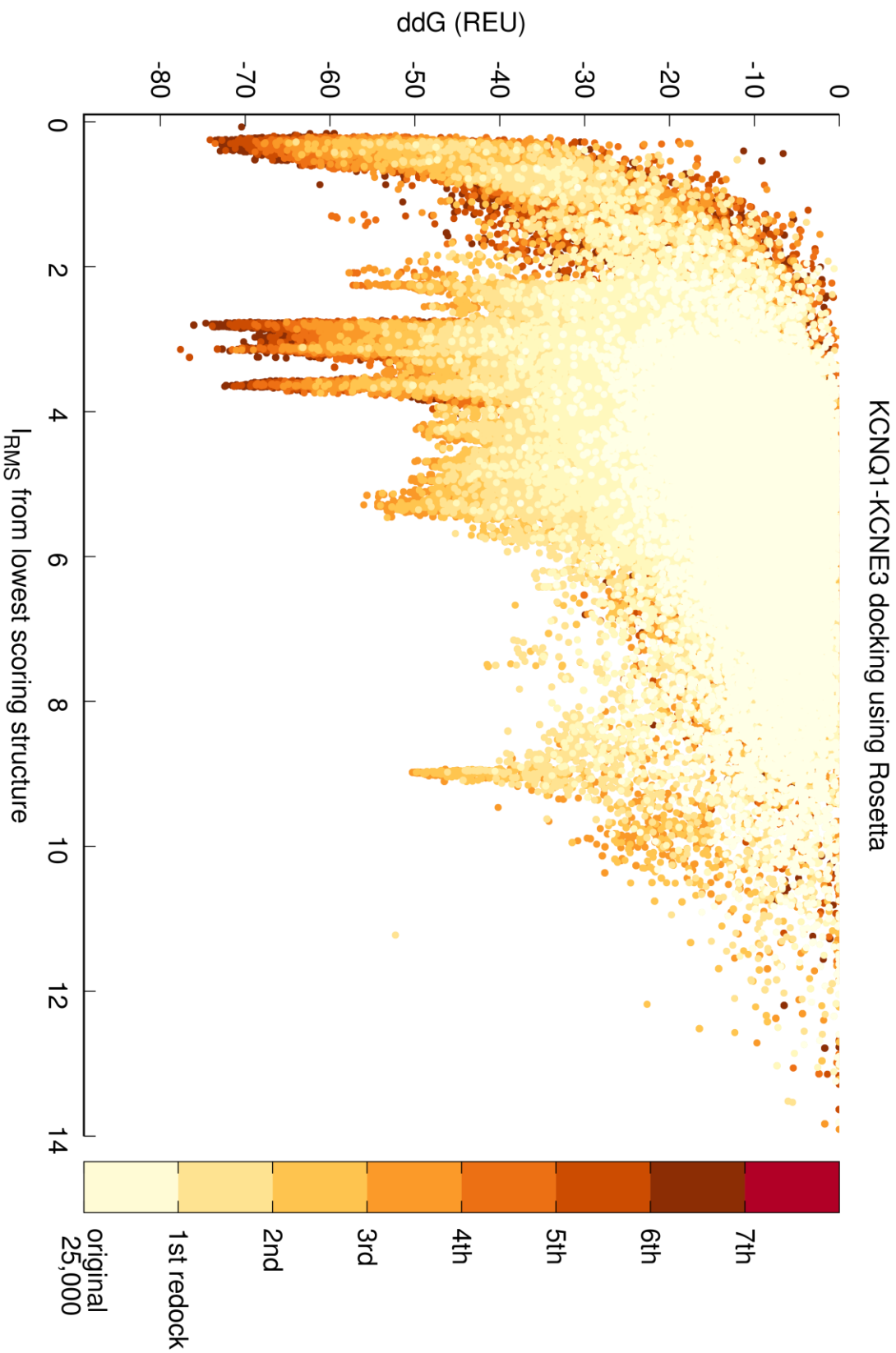

fig. S13. Calculated binding energies (ddG) versus interface root mean squared deviation (I_{rms}) of interface α-carbon positions compared to the lowest-scoring KCNE3-KCNQ1 (open) complex. The color reflects the docking iteration number. Early iterations did not discriminate between the conformations generated. However, after the fifth redocking step, a docking funnel is observed.

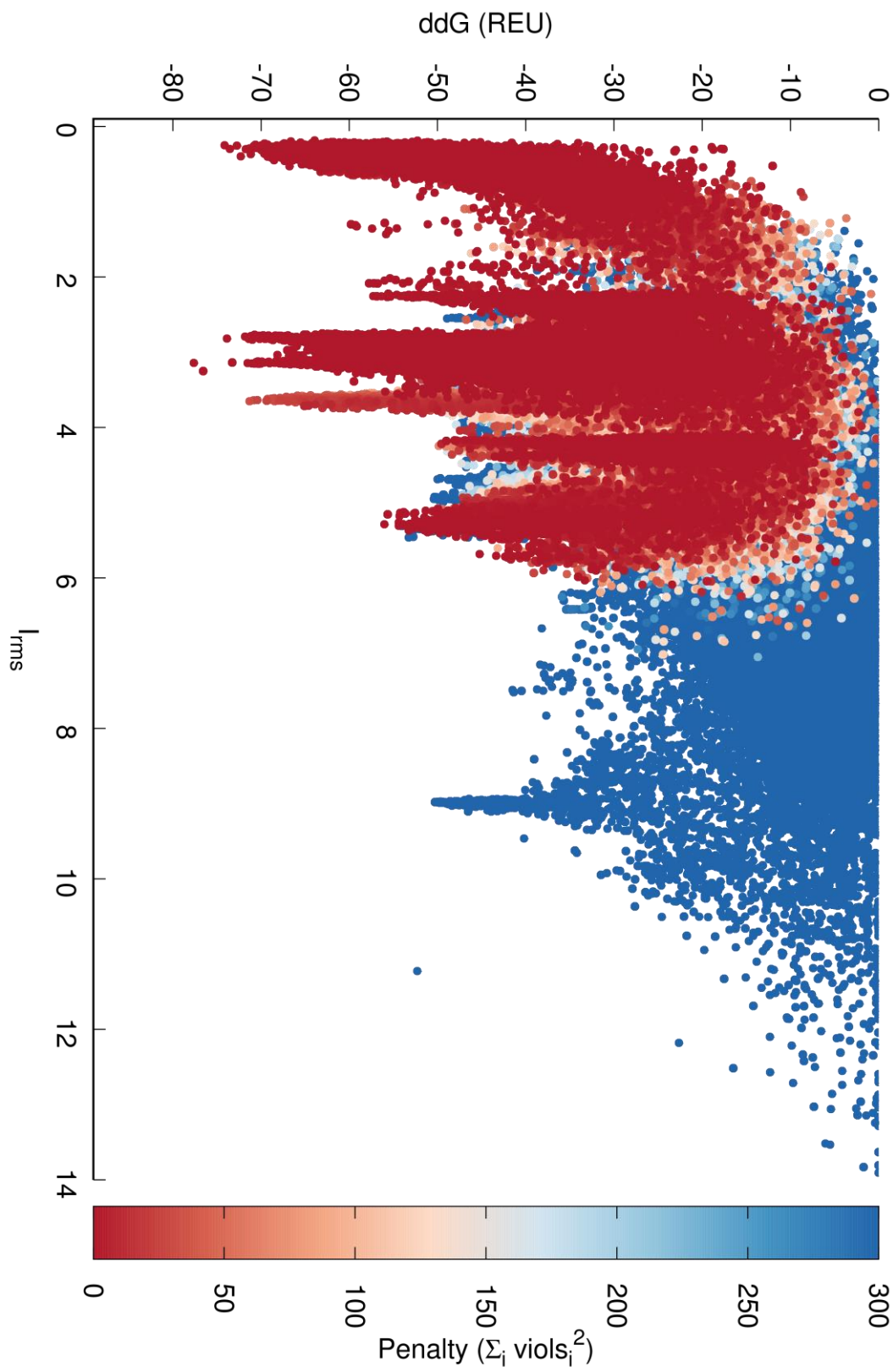

fig. S14. Same plot as fig. S13 with color displaying the total distance restraint violations. All docked complexes are represented, including complexes with distance restraint (a_p_c) violations in excess of 250.

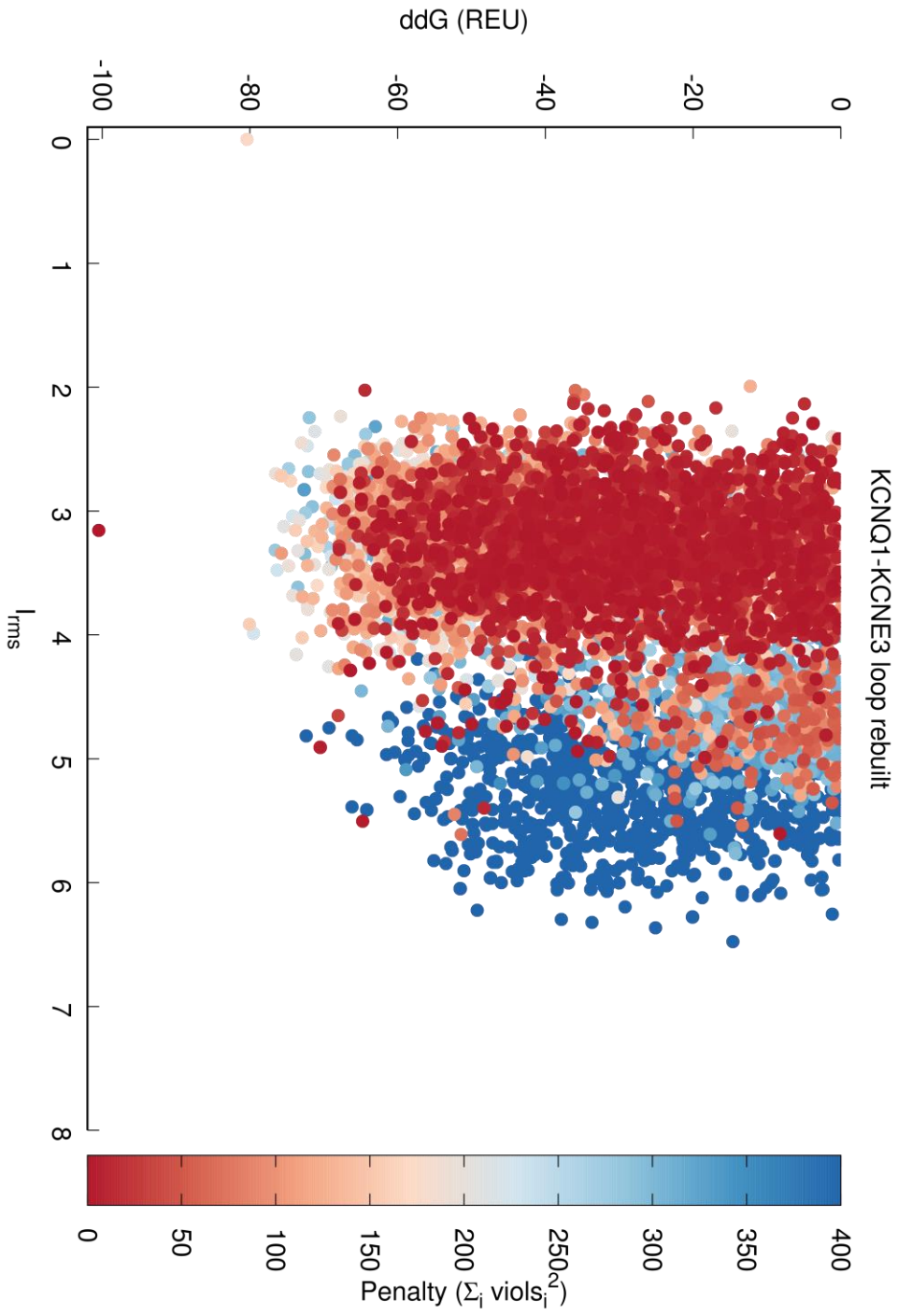

fig. S15. Rebuilding flexible regions within the KCNQ1-KCNE3 complex. Binding energy (ddG) vs. interface rmsd of the best scoring, docked complexes with flexible regions rebuilt and colored based on distance restraint violation.

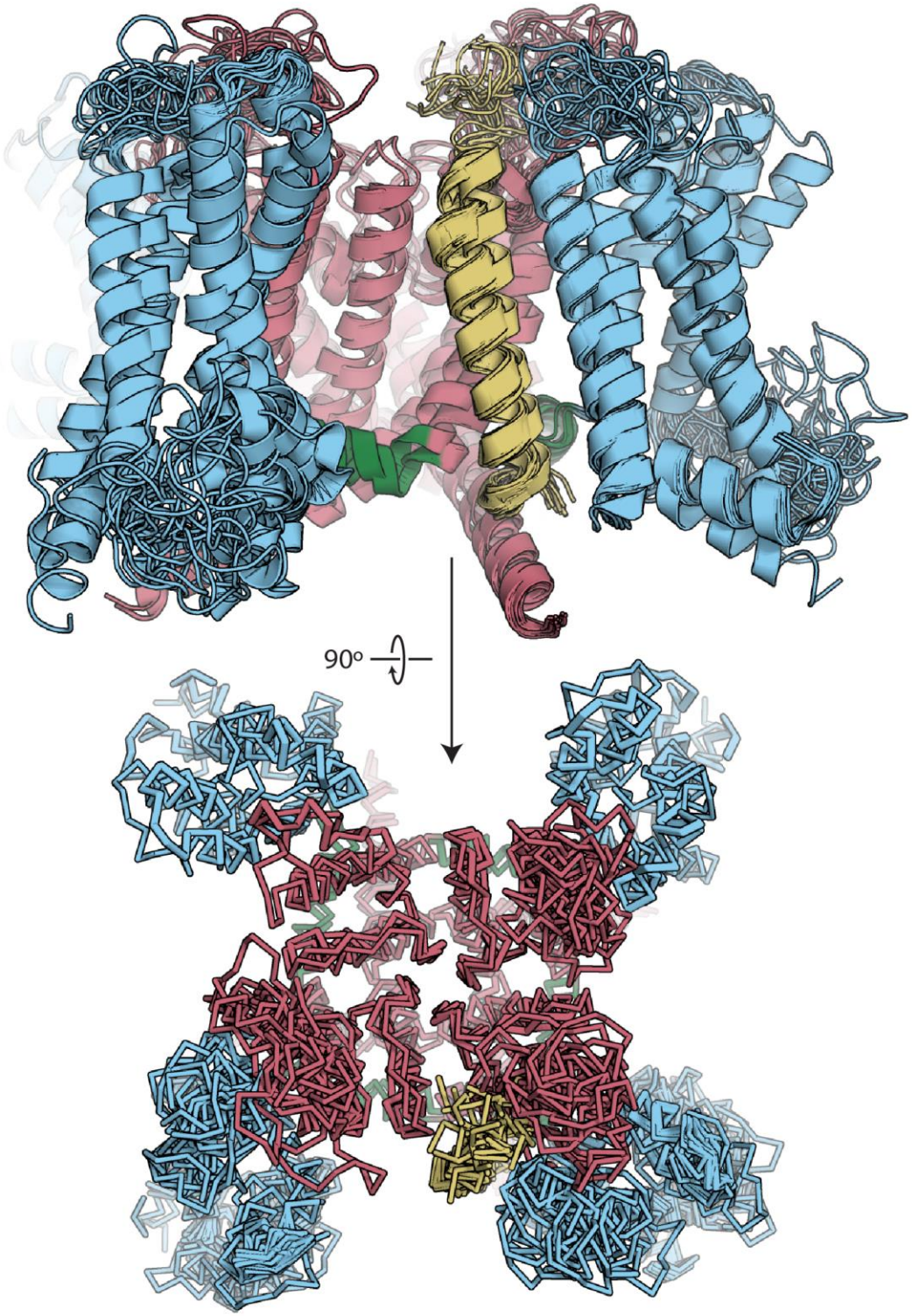

fig. S16. Representative 23 KCNE3-KCNQ1 models based on satisfaction of experimental restraints and Rosetta scoring function.

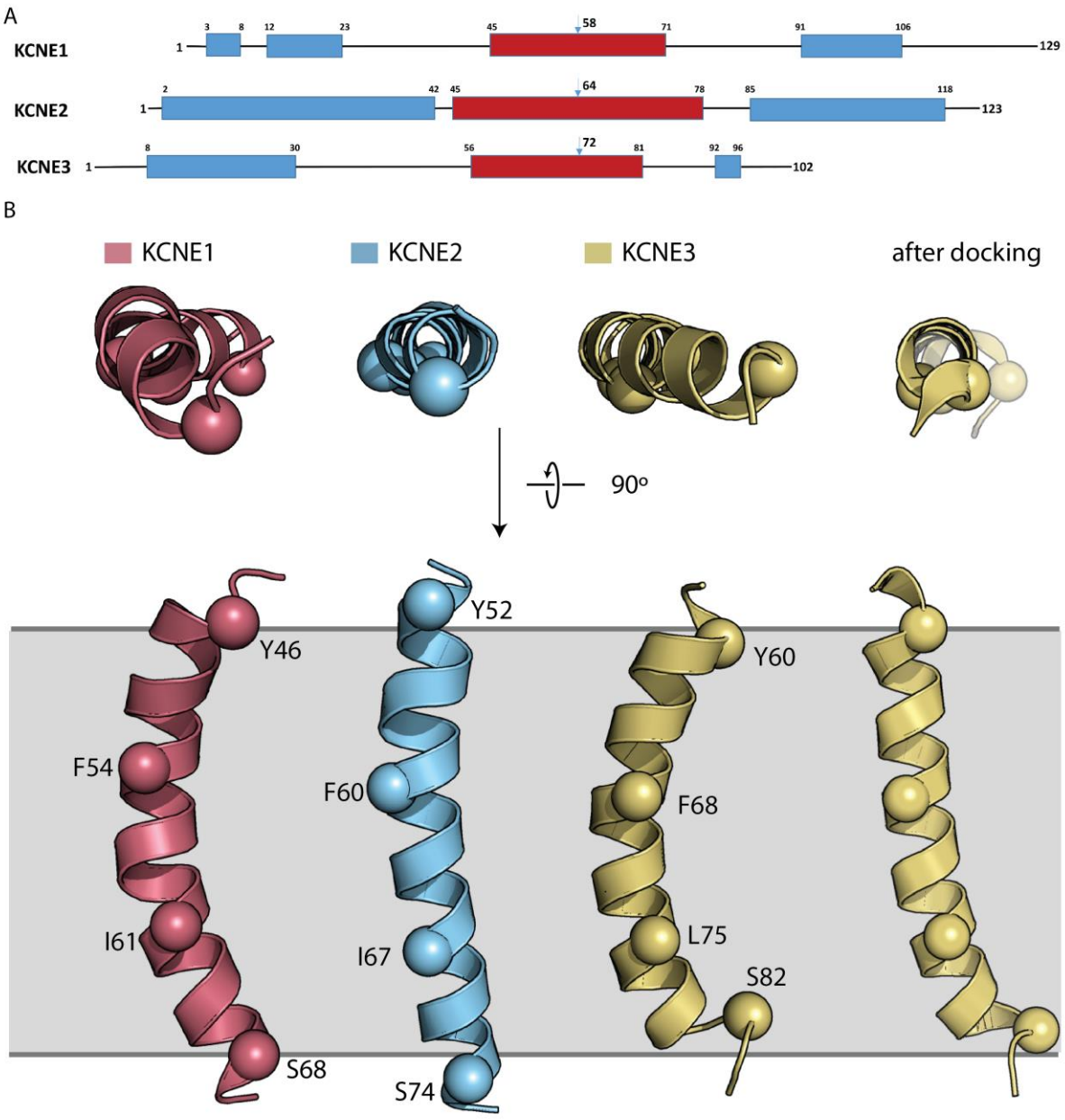

fig. S17. Comparison between structurally characterized KCNE family members. (A) Cartoon comparisons of the locations of the helical segments in KCNE1, KCNE2 and KCNE3 (B) Overlay of the experimentally-determined structure of the transmembrane domains of KCNE1, KCNE2 and KCNE3. KCNE1 and KCNE2 structures (PDB codes 2K21 and 2M0Q, respectively) were determined in previous studies (*2, 27*).

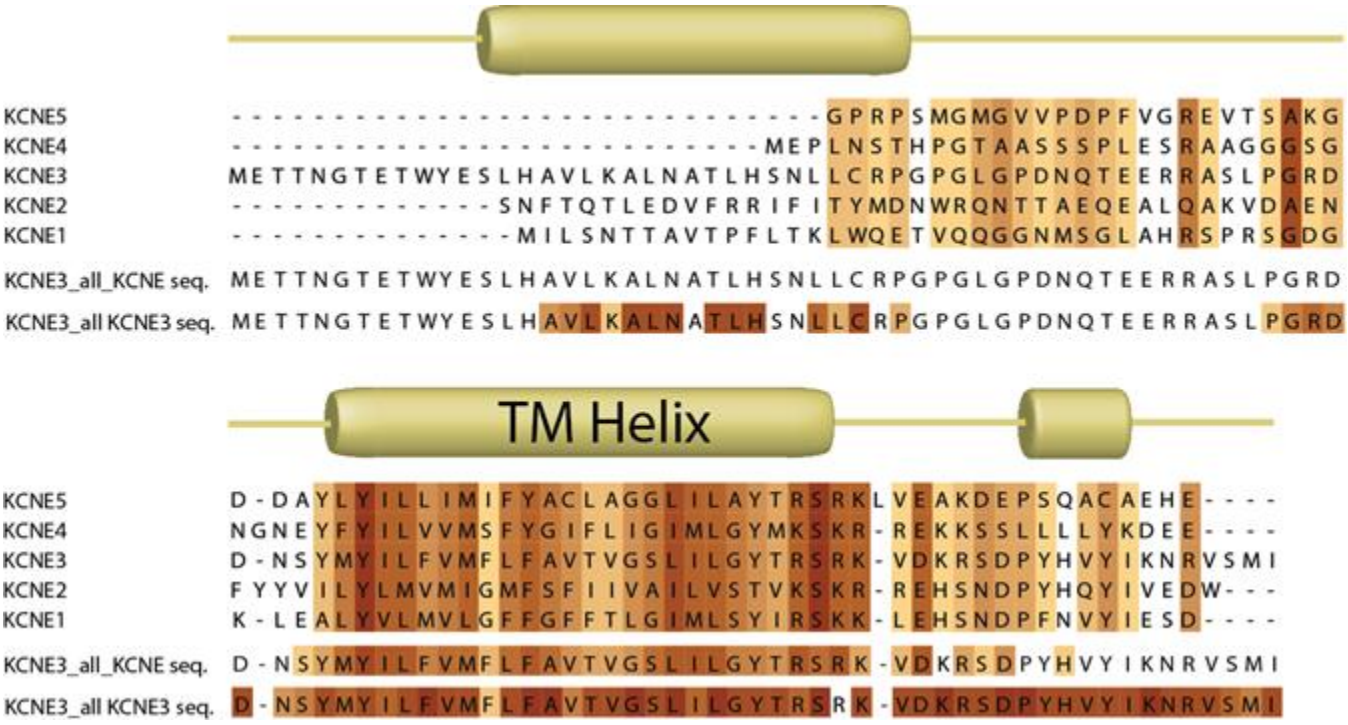

fig. S18. Sequence conservation within the entire KCNE family and within KCNE3 from different organisms. Sequence boxes are color-coded from white (divergent) to dark red (conserved) residues, respectively. Human KCNE family members 1-5 are aligned and color coded to each other in the top two-thirds of the plot. The bottom two sequences include *all* known KCNE family members or all known KCNE3 sequences, upper and lower, respectively. The secondary structure of KCNE3 as determined in this work is shown at the top of this figure.

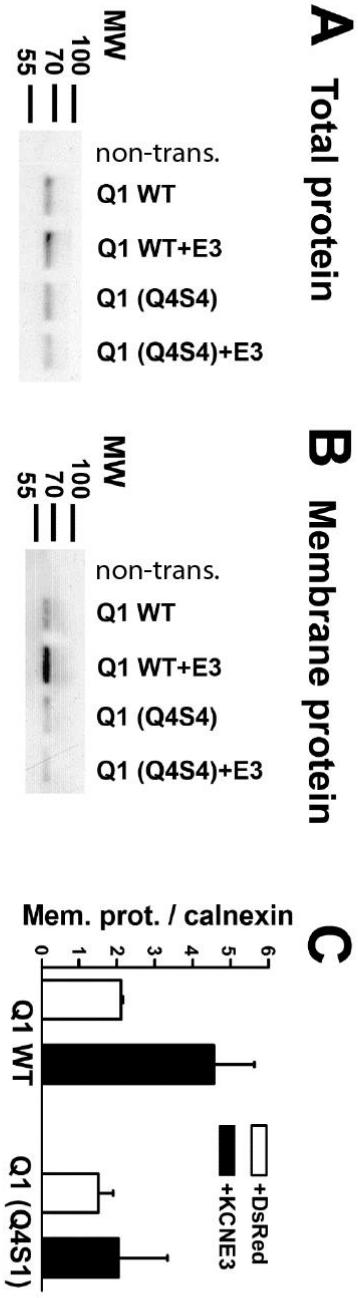

fig. S19. KCNE3 reduces the KCNQ1[Q4S4] current amplitude without reducing channel protein levels at the membrane. Total (**A**) and cell surface (**B**) protein isolated from CHO cells transiently expressing KCNQ1-WT (Q1_WT) or KCNQ1[Q4S4]. (**C**) Densitometric analysis of total and cell surface KCNQ1 from two batches of transfected CHO cells.

Supplementary Tables

table S1. Statistics for restraints, structural calculations, and structural quality for the 10 lowest-energy structures of 9764 calculated using XPLOR and further refined in AMBER.

NMR distance and dihedral and RDC restraints		
Distance restraints	304	
Total NOE	189	
Inter-residue	189	
Sequential (|i-j| = 1)	110	
Medium-range (|i-j| < 4)	79	
Long-range (|i-j > 5)	0	
PRE restraints**	*84*	
Hydrogen bonds	31	
Total dihedral angle restraints	196	
Phi	98	
Psi	98	
RDC restraints in neutral gel	39	
Structure statistics	**Xplor-NIH**	**Amber***
Violations (mean and s.d.)		
Distance constraints (Å)	0.047±0.001	0.041±0.006
Dihedral angle constraints (°)	0.87±0.02	22±4***
RDC (Hz)	0.58±0.02	3.6±0.4
Max. dihedral angle violation (°)	5.544	***
Max. distance constraint violation (Å)	0.0	0.0
Average C_α pairwise r.m.s.d. (Å)		
N-terminal Helix (11-30)	0.958	1.439
Transmembrane Helix (56-82)	0.209	0.994
Ramachandran plot (%)		
Most favored regions	89.4	88.2
Additionally allowed regions	10.2	11.8
Generous allowed regions	0.0	0.0
Disallowed regions	0.0	0.0

* 10 representative NMR structures were used in docking calculations

** From each mutant, we obtained different numbers of PRE-based distances: Ser13Cys (11), Ser57Cys (20), Ser74Cys (30), and Ser82Cys (23).

*** Dihedral angles oscillated around the experimental value, especially in unstructured loops, to yield the large violations observed in any single structure.

table S2. KCNQ1-KCNE3 residue pairs predicted to be proximal based on experimental work.

KCNQ1 residue/s	*KCNE3 residue/s*	*Distant Restraint (Å)*	*Distance in Final Docked Complex* (Å)*	*Reference*	*Related Experimental Data*	*Cells*
240	Any	< 11	8.2	This manuscript	mutations disrupt KCNE3 modulation of channel function	CHO
241	Any	< 11	4.0	This manuscript	mutations disrupt KCNE3 modulation of channel function	CHO
244	Any	< 11	2.0	This manuscript	mutations disrupt KCNE3 modulation of channel function	CHO
142	59	< 17	10.2**	This manuscript	S-S bond formation reduced current, presumably induced conformation change	CHO
244	82	< 17	9.1	This manuscript	S-S bond formation reduced current, presumably induced conformation change	CHO
228	54 or 55	< 5	6.1	Barro-Soria et al. 2015 (28)	mutagenesis and voltage clamp fluorimetry	Oocytes
123, 127, and 130	Any	< 17	3	Nakajo et al. 2011 (29)	lowered current and delayed opening, presumably lowered binding affinity	Oocytes
237	54 or 55	<10***	13.4	Choi et al. 2010 (30)	double mutant thermodynamic cycle analysis	Oocytes
338	72	<17***	17.9	Panaghie et al. 2006 (31)	double mutant thermodynamic cycle analysis	Oocytes

*****Closest contact between any pair of atoms in the specified pair of KCNE3 and KCNQ1 residues.
** C_α - C_α distance
*** Not employed as a restraint in the final docking calculations. However, the resulting top scoring integrative model obtained in calculations in which these restraints were employed was similar to the final model presented in this work that was developed when these restraints were not used. See Results section of main paper for additional discussion.